



CERN-EP-2023-267
20 November 2023

Common femtoscopic hadron-emission source in pp collisions at the LHC

ALICE Collaboration*

Abstract

The femtoscopic study of pairs of identical pions is particularly suited to investigate the effective source function of particle emission, due to the resulting Bose–Einstein correlation signal. In small collision systems at the LHC, pp in particular, the majority of the pions are produced in resonance decays, which significantly affect the profile and size of the source. In this work, we explicitly model this effect in order to extract the primordial source in pp collisions at $\sqrt{s} = 13$ TeV from charged π – π correlations measured by ALICE. We demonstrate that the assumption of a Gaussian primordial source is compatible with the data and that the effective source, resulting from modifications due to resonances, is approximately exponential, as found in previous measurements at the LHC. The universality of hadron emission in pp collisions is further investigated by applying the same methodology to characterize the primordial source of K–p pairs. The size of the primordial source is evaluated as a function of the transverse mass (m_T) of the pairs, leading to the observation of a common scaling for both π – π and K–p, suggesting a collective effect. Further, the present results are compatible with the m_T scaling of the p–p and p– Λ primordial source measured by ALICE in high multiplicity pp collisions, providing additional evidence for the presence of a common emission source for all hadrons in small collision systems at the LHC. This will allow the determination of the source function for any hadron–hadron pairs with high precision, granting access to the properties of the possible final-state interaction among pairs of less abundantly produced hadrons, such as strange or charmed particles.

*See Appendix B for the list of collaboration members

1 Introduction

Femtoscopy is a technique of connecting the pair-wise momentum correlations to the properties of particle emission and the subsequent final-state interaction (FSI) [1, 2]. This formalism is often applied to identical charged pions in order to study the effective source function of particle emission. This is achieved by taking advantage of the Bose–Einstein correlation signal present in the same-sign $\pi\text{--}\pi$ system. These techniques are quite advanced in heavy-ion collisions, for which the source function is well described by a Gaussian parameterization and the corresponding source size shows a distinct decrease as a function of the pair transverse mass (m_T). The latter is commonly referred to as m_T scaling and typically attributed to the presence of collective phenomena, i.e. radial flow [1], and is well described by models with a hydrodynamic phase [3–5]. Recently, femtoscopic studies in small collision systems, pp in particular, have gained a lot of attention due to the possibility of producing pairs with low relative momentum at distances comparable to the range of the strong force ($\approx 1\text{--}2$ fm). The signal related to the FSI, embedded in the measured correlation function, allows for testing of theoretical predictions as well as extracting information about the low-energy scattering parameters, such as the scattering length and effective range. Nevertheless, the successful application of this technique requires the source function to be well constrained. The ALICE Collaboration has demonstrated that a common emission of primordial baryons, i.e. particles produced during the initial collision, is present in pp collisions by analyzing p–p and p– Λ correlations [6]. Similar to heavy-ion collisions, the results in pp collisions show a clear m_T scaling, the nature of which is not yet understood. While hydrodynamic models are well motivated and established for heavy-ion collisions [7], this is not the case for pp collisions where there is controversy on the matter. The modeling of the source is realized with the so-called Resonance Source Model (RSM) [6], which assumes a universal Gaussian core for all primordial particles and accounts for hadron production through resonances, finally yielding an effective source. The abundances of resonances are obtained from the statistical hadronization model [8], assuming a canonical ensemble, while the specific decay kinematics can be extracted from a transport model, e.g. EPOS [9]. This opened the possibility to test for the first time both lattice QCD predictions for the more rare pairs p– Ξ and p– Ω [10], to probe the coupled-channel dynamics for $K^-\text{--}p$ [11], to constrain the chiral effective field theory using the p– Λ [12] and $\Lambda\text{--}\Xi$ [13] channels, and to access the interaction of a vector meson with baryons through $\phi\text{--}p$ [14]. Although the m_T scaling is not explicitly modeled within the RSM, an independent analysis employing a new framework, called CECA [15], relates the m_T scaling to the radial expansion of the collision system.

The goal of this work is to explore if the ansatz of a common source can be extended to the meson–meson and meson–baryon sectors. This is achieved by employing the RSM to extract the effective Gaussian size of the same-sign primordial $\pi\text{--}\pi$ ($\pi^+\text{--}\pi^+$ and $\pi^-\text{--}\pi^-$) and $K\text{--}p$ ($K^+\text{--}p$ and $K^-\text{--}\bar{p}$) sources as a function of m_T , and investigate if they are compatible with the p–p source extracted from the same data set collected from high-multiplicity pp collisions at $\sqrt{s} = 13$ TeV. In this way, the assumption of a universal hadron emission in small collision systems will be solidified. Furthermore, as the found m_T scaling is currently not understood, the additional information on the source size at very low- m_T (< 1 GeV/ c^2) will provide valuable information for transport [9, 16] and effective source [15] models. Finally, we perform the $\pi\text{--}\pi$ correlation analysis in minimum-bias (MB) events using three different multiplicity classes in order to provide even more differential data.

The article is structured as follows. In Sec. 2 details regarding the data analysis are given, in particular about the particle identification using the ALICE detector. This is followed by a brief review of the femtoscopic method in Sec. 3, which includes the model used for fitting the experimental correlation functions. The source function for the studied pairs is discussed in Sec. 4, which entails an investigation on the modification of the source function due to short-lived resonances. Section 5 focuses on the obtained results, which are then discussed within the context of recent measurements. Finally, a summary is given in the closing Sec. 6.

2 Data analysis

The data analyzed in this work were collected by the ALICE Collaboration [17] at the LHC in pp collisions at $\sqrt{s} = 13$ TeV. Additional details on the ALICE detector setup can be found in [18]. In this analysis, the following main subdetectors are used: the V0 detectors [19], the Inner Tracking System (ITS) [20], the Time Projection Chamber (TPC) [21], and the Time-Of-Flight (TOF) detector [22]. Events passing a MB trigger are selected by requiring coincident signals in both V0 [19] detectors to be synchronous with the beam crossing time defined by the LHC clock. High-multiplicity (HM) events are selected online by applying a threshold on the amplitude of the signal in the V0 detectors in addition to the MB trigger conditions. The V0 detectors consist of two arrays of plastic scintillators, one located at forward ($2.8 < \eta < 5.1$) and the other placed at backward ($-3.7 < \eta < -1.7$) pseudorapidity [19]. The measured amplitudes within these scintillators are used to define multiplicity classes for events. Additional measurements at midrapidity, utilizing the innermost layers of the ITS, then provide estimates for the average charged particle multiplicity at mid-pseudorapidity ($\eta=0$) in a unit interval of pseudorapidity $\langle dN/d\eta \rangle_{|\eta|<0.5}$ in a given multiplicity class. This procedure allows one to associate $\langle dN/d\eta \rangle_{|\eta|<0.5}$ with a V0-based multiplicity class. For the HM case, the selected events correspond to the 0.17% highest multiplicity inelastic pp collisions with at least one charged particle in the range $|\eta| < 1$ (referred to as INEL > 0) [17, 18]. The resulting HM data sample contains events with an average multiplicity of approximately 30 charged particles in the pseudorapidity interval $|\eta| < 0.5$ [10]. Events with multiple primary vertices, identified from track segments in the two innermost layers of the ITS, are tagged as pile-up and removed from the analyzed sample.

The charged-particle tracking and the primary vertex (PV) reconstruction are obtained using the combined track information of the ITS and TPC [17], located inside a uniform magnetic field of 0.5 T directed along the beam direction. A selection of ± 10 cm on the deviation between the z coordinate of the reconstructed PV and the nominal interaction point is applied to ensure a uniform detector coverage in the pseudorapidity region of $|\eta| < 0.8$. The quality of the tracks used for the construction of the π - π (K-p) correlation is ensured by requiring that each track lies within the pseudorapidity range of $|\eta| < 0.8$ while also requiring that a minimum of 80 (70) clusters in the TPC [21] are assigned to each track. Further quality assurance is provided by requiring that at least 70 out of the total of 159 rows of the TPC readout pads are crossed in conjunction with finding clusters in at least 80% of these crossed rows. For this analysis, different transverse momentum ranges for the tracks were considered depending on the particle species and the particle-identification (PID) capabilities of ALICE. For pions, protons and kaons these ranges are $0.14 < p_T < 4$ GeV/c, $0.8 < p_T < 3$ GeV/c, and $0.4 < p_T < 1.4$ GeV/c, respectively. The PID for the charged pions, kaons, and protons is performed using the TPC and TOF detectors. The deviation of the measured TPC response to the Bethe-Bloch parameterization of $\langle dE/dx \rangle$ for the mass hypothesis of the considered particle is expressed as multiples of the standard deviation n_σ , determined by the resolution of the TPC. For pions, only those tracks satisfying $|n_{\sigma,\text{TPC}}| < 3$ for a transverse momentum $p_T < 0.5$ GeV/c are further analyzed. In the range $p_T > 0.5$ GeV/c, the pion specific energy loss band overlaps with those of kaons and protons. Hence, up to $p_T < 4$ GeV/c, also the TOF information is used. The difference between the measured TOF response and the velocity calculated for a pion as a function of the momentum is expressed as $n_{\sigma,\text{TOF}}$, and combined with the TPC information into $n_{\sigma,\text{combined}} = (n_{\sigma,\text{TPC}}^2 + n_{\sigma,\text{TOF}}^2)^{(1/2)}$. Only tracks satisfying $|n_{\sigma,\text{combined}}| < 3$ are further analyzed. The selection for charged kaons (protons) is described in [11] and follows the same strategy for PID used for the charged pions. For 0.15 (0.4) $< p_T < 0.4$ (0.8) GeV/c only TPC information is used, and the $|n_{\sigma,\text{TPC}}| < 3$ criterion is applied. Again, the combined TPC and TOF information is used for 0.4 (0.8) $< p_T < 1.4$ (3) GeV/c and required to be less than 3 times of $n_{\sigma,\text{combined}}$. In order to remove a large fraction of the e^\pm contamination of the $\langle dE/dx \rangle$ bands of charged kaons (protons), the identified particle candidates were excluded in the region of 0.3 (0.6) $< p_T < 0.4$ (0.8) GeV/c. As it was shown in Refs. [11, 23], this selection does not introduce any bias to the correlation function.

For femtoscopic studies, the primary particles, which experience the final-state interaction, are of special interest, and the amount of secondary (feed-down) particles stemming from weak decays and interactions in the detector material have to be suppressed. This is achieved by requiring that the distance-of-closest approach (DCA) to the primary vertex of the tracks used for the π - π (K-p) correlation is less than 0.3 (1.0) cm in the transverse and longitudinal planes with respect to the beam direction.

The two-particle correlation function is measured as a function of the relative momentum ($k^* = \frac{1}{2}|\vec{p}_1^* - \vec{p}_2^*|$), where all quantities, denoted with an asterisk (*), are evaluated in the rest frame of the particle pair (PRF). The momentum in the PRF of particle i is denoted by \vec{p}_i^* . The measured correlation function contains in principle all correlations imprinted on the relative momentum (k^*) distribution regardless of the origin, consequently the background has to be taken into account. This correlated residual background stems from hard partonic interactions in the initial stage of the collision, and leads to highly correlated particles in jet-like structures, leading typically to less isotropic events. For the analysis of the correlation functions of π - π pairs from MB events and of K-p pairs from HM events, a selection based on the event shape observable called transverse sphericity [24, 25] $S_T > 0.7$ is applied in order to suppress the mini-jet background, largely present in pp collisions [11, 14, 25–28]. No selection on the sphericity is applied in the case of π - π correlations for the events in the HM sample because these events are typically more spherical, and because the selection of $S_T > 0.7$ affects the relative momentum correlation function of π - π pairs, mostly for $k^* > 500$ MeV/c, which is well outside the signal region of $k^* < 250$ MeV/c. After applying the event selection criteria, the analyzed sample consists of about 10^9 MB and 10^9 HM events.

For tracks close in phase space, reconstruction errors can occur in the form of track merging or splitting [29]. Therefore, an additional selection for the close-pair rejection is included by imposing a circular cut on the relative angular separation measured by the relative pseudorapidity $\Delta\eta$ and azimuthal angle $\Delta\phi^*$, $\sqrt{\Delta\phi^{*2} + \Delta\eta^2} < (1 \times 10^{-2})$ of the tracks, hence, demanding a minimum separation. Here $\Delta\phi^*$ is corrected for the change in azimuthal angle induced by the magnetic field. The use of this selection completely removes the signatures of track merging or splitting.

The purity of the PID selections and the contamination due to weak decays (feed-down) of the sample were studied with the help of Monte Carlo (MC) simulations using PYTHIA 8.2 [16] (Monash 2013 Tune) generated events, which were transported by GEANT 3 [30] through the ALICE detector and subsequently processed by the reconstruction algorithm [17]. The purity has been studied as a function of p_T , nevertheless a negligible dependence, even across the threshold at which the TOF information is used, was observed. The p_T averaged purity obtained with the PID selections described above is about 99% for charged pions, kaons, and protons. The primary and secondary fractions are obtained by extracting from the MC the template distributions of the DCA in the transverse plane and fitting these to the measured distributions. The information about the purity and composition of the sample is crucial for femtoscopic studies and is used to determine the λ parameters, which are introduced in Sec. 3.

The correlation function is studied differentially in intervals of the pair transverse mass m_T , which is connected to the average transverse momentum of the particle pair ($k_T = \frac{1}{2}|\vec{p}_{T1} + \vec{p}_{T2}|$) via the relation $m_T = (k_T^2 + m_{\text{avg}}^2)^{(1/2)}$, where m_{avg} is the average mass of the studied particle pair. The π - π correlations are studied in five (0.15–0.30, 0.30–0.50, 0.50–0.70, 0.70–0.90, 0.90–1.50 GeV/c) k_T ranges for the MB and HM datasets. The K-p correlations are studied in four (1.2–1.4, 1.4–1.5, 1.5–1.8, 1.8–2.0 GeV/c²) m_T ranges in HM collisions.

The systematic uncertainties of the correlation function associated with the choice of the selection criteria are estimated by performing the selection 44 times while varying randomly the track selection and PID criteria (i.e. p_T boundaries at which TOF is used and the $n\sigma$ threshold) by 20% and excluding the S_T selection from the procedure. The choice of including no variation on S_T was made to ensure that the same events are always used as input in the analysis. In order to ensure that the observed deviation with

respect to the default settings does not originate from statistical fluctuations, only variations for which the yield of pairs for $k^* < 200$ GeV/c does not exceed 20% compared to the yield obtained from the default settings are used. The magnitude of the uncertainty is estimated using the root-mean square deviation for a uniform distribution in each k^* interval, using the underlying uniform distribution obtained from the 44 variations.

3 Two-particle correlations

The observable of interest in femtoscopic studies is the two-particle correlation function $C(k^*)$, measured as a function of k^* . Experimentally, $C(k^*)$ is calculated from the normalized ratio

$$C(k^*) = \mathcal{N} N_{\text{same}}(k^*) / N_{\text{mixed}}(k^*), \quad (1)$$

where $N_{\text{same}}(k^*)$ is the distribution of k^* obtained from particles produced in the same event, and $N_{\text{mixed}}(k^*)$ is the k^* distribution of uncorrelated pairs. The latter is generated using the mixed event technique [1], for which a pair is built by selecting particles from different events. To avoid any bias pertaining to reconstruction efficiencies or acceptance, only identified particles are used from events for which the difference in the z coordinate of the reconstructed primary vertex is less than 2 cm and the difference in dN_{ch}/dy at midrapidity ($|y| < 0.5$) is less than 4. The normalization \mathcal{N} is calculated in $k^* \in [350, 400]$ MeV/c, in which no femtoscopic signal is present, and the theoretical value of $C(k^*)$ approaches unity. In order to extract the source parameters a femtoscopic fit is performed using a model for the expected theoretical correlation function.

The theoretical definition of $C(k^*)$ is given by the Koonin–Pratt equation [1]

$$C(k^*) = \int d^3 r^* S(r^*) |\psi(r^*, k^*)|^2, \quad (2)$$

and depends on the source function $S(r^*)$, which encodes the relative distance r^* in the PRF, and the two-particle relative wave function $\psi(r^*, k^*)$. In this work, the latter is obtained by employing the "Correlation Analysis Tool using the Schrödinger Equation" (CATS) framework [31], which numerically solves the Schrödinger equation for a configurable interaction potential. In the case of the π – π pairs, the wave function is determined by quantum statistics and Coulomb repulsion. For the K–p correlations, the strong interaction is modeled assuming state-of-the-art chiral potentials [23, 32], while the Coulomb interaction is directly taken into account using CATS. The shape of $S(r^*)$ follows a convolution of a Gaussian distribution (core) and an exponential function (tail) [6]. The Gaussian core, from which primordial particles are emitted, is fully determined by its width r_{core} and the exponential contribution takes into account the resonance decays to the pair of interest. Further details on the $S(r^*)$ are discussed in Sec. 4. The Koonin–Pratt relation is a subject to several approximations, as discussed in [1]. These approximations have been originally designed for large emission sources, as found in heavy-ion collisions, nevertheless they have been successfully applied in identical pion femtoscopy in p–p collision systems [27, 33, 34].

The measured $C(k^*)$ encompasses not only correlations arising from primordial pairs but also incorporates contributions from weak decays, long-lived resonances (with a proper decay length greater than 5 fm) and misidentified particles. These additional components consist of what are commonly referred to as "feed-down" particles and impurities, and they can be taken into account by the λ parameter formalism, as was shown in [35]. The general form of the modeled correlation function $C_{\text{model}}(k^*)$ is given by

$$C_{\text{model}}(k^*) = 1 + \sum_i \lambda_i (C(k^*) - 1). \quad (3)$$

In this analysis, a decomposition of the correlation function into three components is considered, namely the genuine (gen), the feed-down (feed), and the misidentified candidates (misid), leading to

$$C_{\text{model}}(k^*) = 1 + \lambda_{\text{gen}}(C_{\text{gen}}(k^*) - 1) + \lambda_{\text{feed}}(C_{\text{feed}}(k^*) - 1) + \lambda_{\text{misid}}(C_{\text{misid}}(k^*) - 1). \quad (4)$$

By definition, the sum of the three contributions is normalized to unity [35]. The genuine contribution contains the pairs of primary particles experiencing the final-state interaction and particles stemming from short-lived strongly decaying resonances. Details about the considered resonances are given in the following Sec. 4. The pairs containing at least one particle originating from weak or electromagnetic decays are described by the feed-down component. Finally, the pairs with at least one misidentified particle are quantified by the misidentification part. The latter additionally includes particles which are produced in interactions between the particles produced in the event and the detector material, whose overall contribution is however negligible. The $C(k^*)$ associated with the feed-down and misidentified components are considered to be flat, leading to a simplified form of Eq. (4):

$$C_{\text{model}}(k^*) = \lambda_{\text{gen}} C_{\text{gen}}(k^*) + \lambda_{\text{feed}} + \lambda_{\text{misid}}. \quad (5)$$

The λ_i parameters are evaluated from the single-particle properties as a product of the purity \mathcal{P}_i , determined via MC studies and fractions of primary particles f_i obtained from fits to the experimental DCA distributions in the transverse plane. The formula used for the evaluation is $\lambda_{ij} = \mathcal{P}_i f_i \mathcal{P}_j f_j$, where the indices i and j indicate the origin (in this case primary, feed-down and misidentification) of the single particles which form the pair. The λ_{gen} and λ_{feed} are determined as described above, λ_{misid} is then obtained by the constraint that the sum of the three contributions is normalized to unity, and driven by the purity.

To account for any residual non-femtoscopic background, the function used in the femtoscopic fit to the measured $C(k^*)$ is modified by an additional baseline

$$C_{\text{fit}}(k^*) = B_{\text{non-femto}}(k^*) \times C_{\text{model}}(k^*), \quad (6)$$

where $B_{\text{non-femto}}(k^*)$ is the baseline function of the residual non femtoscopic background. In the case of same-sign pions, two functions for the baseline are tested, a polynomial of first and second degree, while for the K-p correlations a constant, a first, and a second order polynomial are considered. In π - π correlations from the MB sample, a residual mini-jet background is also present after applying the sphericity selection. Hence, to remove this remaining non-femtoscopic component, the $C(k^*)$ obtained from MB data is divided by the correlation function obtained from MC before using it in the femtoscopic fit. The same strategy was already employed by the ATLAS and CMS Collaborations [33, 34]. The typical size of this correction is around 10%. The free parameters of the fit are the baseline parameters, and the width r_{core}^* of the source function. The fit is performed in the range of $0 < k^* < 364(270)$ MeV/c for π - π (K-p). A variation of $\pm 10\%$ in the upper limit of the fitting range is considered to account for any systematic effect related to the range chosen for the fit.

4 Modeling of short-lived resonances

The detailed study of the particle source function $S(r^*)$ for baryon-baryon pairs was presented in [6] and enabled studies of the interaction between many particle pairs, including for example, p- Ω [10]. In

this work, the MC procedure developed in [6] serves as a baseline to determine, for the first time, the emitting source for primordial particles as a function of m_T for meson–meson and meson–baryon pairs.

The source function $S(r^*)$ according to the RSM [6] is a two component ansatz. A Gaussian source is used for primordially produced particles, i.e. initial particles produced in the pp collisions. It has a width r_{core} , called “core source”. The general Gaussian parameterization for the two-particle source is

$$S(r^*) = \frac{1}{(4\pi r_0^2)^{3/2}} \exp\left(-\frac{r^{*2}}{4r_0^2}\right), \quad (7)$$

this form is obtained by computing the convolution of two single particle Gaussian sources, each with a respective width of r_0 . In addition to this, the contributions of short-lived strongly-decaying resonances can be parameterized by introducing exponential tails, the so-called “resonance halo”. The analytical determination of the full shape of the source is challenging, because of the kinematics of decaying resonances. Therefore, a MC procedure is employed to access numerically the source function, which can be parameterized by folding the Gaussian in Eq. (7) with the sum of the exponential decay functions for every resonance. The decay kinematics is obtained by extracting the angular distribution of particles emitted from the strong decay of the short-lived resonances from the EPOS [9] model version 3.117, which is configured to simulate MB pp collisions at $\sqrt{s} = 13$ TeV with relativistic hydrodynamics and hadronic UrQMD afterburner enabled. In previous studies [33, 34, 36], the effect of resonances was not explicitly taken into account, instead a Cauchy/Exponential type source parameterization [37] was used

$$S(r^*) = \frac{1}{\pi^2} \frac{r_{\text{exp}}}{(r_{\text{exp}}^2 + r^{*2})^2}. \quad (8)$$

where the size of the source is denoted by r_{exp} .

Within the RSM, the abundances of strongly decaying resonances contributing to the yield of a specific particle are constrained by calculations based on a canonical implementation of the statistical hadronization model (SHM) [38]. For charged pions, kaons, and protons, the THERMAL-FIST [38] package is employed to perform the calculations. The model parameters are evaluated following the procedure described in [39], separately for MB and HM collisions. According to these calculations, around 28% of the charged pions are primordial, while 72% stem from strongly decaying resonances. For charged kaons (protons) the primordial fraction is 52 (36)%. The resonances which contribute at least 1% to the yield of the charged pions and kaons are listed in Tables 2 and 3, respectively, while the detailed decomposition of the proton resonances can be found in Ref. [6]. The mass and lifetime of each strongly decaying resonance are embedded in two effective parameters $\langle m_{\text{res}}^{\text{eff}} \rangle$ and $\langle c\tau_{\text{res}}^{\text{eff}} \rangle$, which are the average mass and decay length computed using as weights the abundances and lifetimes of the considered resonances. As the difference in the relative contribution of resonances is negligible between MB and HM events, in both cases, the same values for the effective parameters are used. The parameters used for the calculations are reported in Table 1 for the MB collisions. The results of these calculations are $\langle m_{\text{res}}^{\text{eff}} \rangle = 1.124$ GeV/ c^2 and $\langle c\tau_{\text{res}}^{\text{eff}} \rangle = 1.5$ fm for the charged pions and $\langle m_{\text{res}}^{\text{eff}} \rangle = 1.05$ (1.36) GeV/ c^2 and $\langle c\tau_{\text{res}}^{\text{eff}} \rangle = 3.66$ (1.65) fm for the charged kaons (protons). Long-lived ($c\tau > 5$ fm) resonances are excluded from the calculation of these average values, as explained in the next paragraph. Along with the decay kinematics obtained by selecting a particle cocktail of matching $\langle m_{\text{res}}^{\text{eff}} \rangle$ and $\langle c\tau_{\text{res}}^{\text{eff}} \rangle$ from events generated with EPOS, all ingredients needed for the RSM are determined. Due to the averaging of the resonance properties it is possible that especially for low k_T pion pairs the $\langle m_{\text{res}}^{\text{eff}} \rangle$ and $\langle c\tau_{\text{res}}^{\text{eff}} \rangle$ are overestimated. However, this is accommodated by including a systematic variation of both parameters. A variation of $\pm 10\%$ for $\langle m_{\text{res}}^{\text{eff}} \rangle$ and $\langle c\tau_{\text{res}}^{\text{eff}} \rangle$ is considered for the fits to account for any systematic effects related to the hadronic cocktail obtained from the SHM as well as the averaging. This procedure may be improved upon, in the future, by simulating each decay independently; first steps in this direction

Table 1: Model specifications and values of parameters used for the yield calculations with THERMAL-FIST [38].

Ideal HRG model specifications	
Ensemble	Canonical
Statistics	Quantum statistics for all particles
Resonance shape	rel. Breit-Wigner distribution
Parameter	Value
Temperature (MeV)	171.0
Strangeness suppression factor	$\gamma_S = 0.78$
Source radius for $ y < 1$ (fm)	$R = 1.58$
Canonical correlated radius (fm)	$R_c = 2.28$
B, Q, S	0

become possible with a new framework handling the particle emission called CECA [15].

Table 2: List of resonances which contribute at least 1% to the yield of π^+ , the contribution of the remaining resonances is summarized by $R_{f<1\%}^\pi$. The fractions are computed with THERMAL-FIST for pp minimum bias collisions at $\sqrt{s} = 13$ TeV and are also used for the high multiplicity sample since the relative abundance of resonances is the same as for minimum bias collisions.

Resonances	Fraction (%)
$\rho(770)^0$	9.0
$\rho(770)^+$	8.7
$\omega(782)$	7.7
$K^*(892)^+$	2.3
$\bar{K}^*(892)^0$	2.6
$b_1(1235)^0$	1.9
$a_2(1320)^+$	1.5
η	1.5
$a_1(1260)^+$	1.4
$f_2(1270)$	1.4
$a_0(980)^+$	1.4
$h_1(1170)$	1.2
$R_{f<1\%}^\pi$	31.4

Table 3: List of resonances contributing at least 1% to the yield of K^+ , the contribution of the remaining resonances is summarized by $R_{f<1\%}^K$. These fractions are computed with THERMAL-FIST for pp high multiplicity collisions at $\sqrt{s} = 13$ TeV.

Resonances	Fraction (%)
$K^*(892)^0$	21.0
$K^*(892)^+$	11.0
$a_0(980)^+$	1.0
$K_2^*(1430)^0$	1.0
$K_1^*(1270)^0$	1.0
$\phi(1020)$	6.0
$R_{f<1\%}^K$	8.0

The result of the RSM for the full π - π source profile, together with the Gaussian core, and an exponential type source profile is shown in the left panel of Fig. 1, while the resulting correlation functions are de-

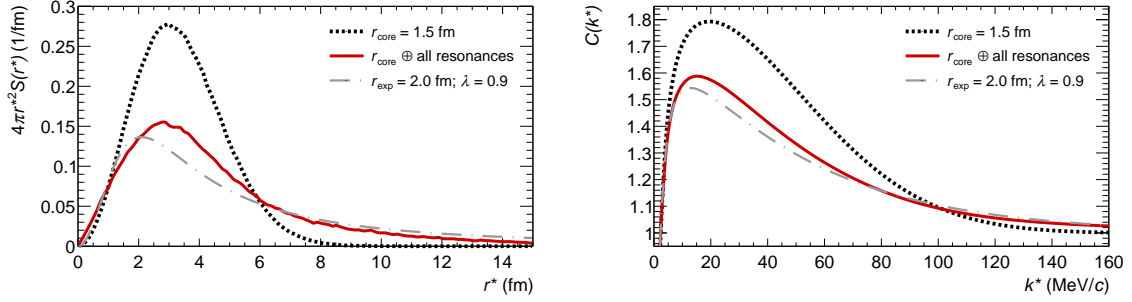


Figure 1: Calculation of the source function (left) and corresponding π - π correlation function (right), performed using CATS [31] employing the RSM. The RSM (full red line) is compared to the usual assumption of an exponential (dash-dotted grey line) source distribution with a radius r_{exp} of the source and a purely Gaussian (dotted black line) source.

picted in the right panel. Comparing the purely Gaussian source, as well as the corresponding correlation function, with the scenario of a source containing exponential tails shows that resonance contributions diminish the overall correlation strength. The Gaussian core source together with the resonance contributions (solid red curve), can effectively be described by an exponential source, scaled by $\lambda = 0.9$ due to contributions of $\approx 10\%$ of long-lived ($c\tau > 5$ fm) strongly decaying resonances (dash-dotted grey curve). Note that $\lambda = 0.9$ can conveniently be absorbed by the usual λ parameters introduced in Eq. (4), especially in the case of a simultaneous fit of the effective source size and λ . The contribution of long-lived resonances ($c\tau > 5$ fm) decaying into charged pions and kaons, such as ω , ϕ , can be considered in the RSM as feed-down from weak decays. In this context, 12.2% (6%) of the charged pions (kaons) can be modeled as secondary particles from weak decays. To take this contribution into account, the λ parameter related to the genuine part has to be corrected for the corresponding abundances of long-lived resonances. The fully corrected λ_{gen} parameters in different k_T (m_T) intervals are presented in Table 4 for π - π and K - p pairs. An uncertainty of 10% has been assigned to the data-driven evaluated values, accounting for possible inaccuracies of the determination of the fractions. The total uncertainty of the analysis is evaluated by employing a bootstrap procedure [40]. This involves two main steps, firstly, randomly sampling from all of the aforementioned systematic variations, secondly, resampling the individual bins of the correlation function based on the statistical uncertainties. Subsequently, the fit procedure is repeated multiple times and a distribution of radii obtained. The central interval of the radii distribution, within which 68% of the mass is concentrated, is calculated and determines the total uncertainty of the analysis. The systematic uncertainty has been isolated by repeating the procedure without resampling for statistical fluctuations. Notably, the dominating source of the systematic uncertainty is the variation of λ parameters, contributing approximately 30% to the total uncertainty.

Table 4: Compilation of λ_{gen} parameters for k_T (m_T) intervals. The values are derived from the fit results of the MC DCA templates to the experimental data, and from purity studies with Pythia 8.2 and GEANT 3 and they are corrected for the abundances of long-lived strongly decaying resonances.

(HM/MB) k_T (GeV/c)	0.15–0.30	0.30–0.50	0.50–0.70	0.70–0.90	0.90–1.50
$\lambda_{\text{gen}}(\pi-\pi)$	0.66 ± 0.07	0.66 ± 0.07	0.66 ± 0.07	0.66 ± 0.07	0.66 ± 0.07
(HM) m_T (GeV/c ²)	1.2–1.4	1.4–1.5	1.5–1.8	1.8–2.0	–
$\lambda_{\text{gen}}(K-p)$	0.76 ± 0.08	0.73 ± 0.08	0.66 ± 0.07	0.65 ± 0.07	–

5 Results and Discussion

The same-sign $\pi\text{--}\pi$ correlation functions in MB collisions are measured in three multiplicity intervals and five different k_T ranges. As an example, correlation functions in the range of k_T (0.50–0.70) GeV/ c and $N_{\text{ch}} > 30$ are shown in Fig. 2. All correlations for the MB dataset are shown in the appendix in Figs. A.1, A.2, and A.3. The systematic uncertainties are represented by boxes. The fits are performed for different k_T and multiplicity classes. On the left (right) panels, the results are shown assuming a polynomial of first (second) degree to describe the baseline of the $C(k^*)$. The strength of the correlation function is sometimes underestimated in the fits with a linear baseline and better accommodated if the second degree polynomial is used to describe the residual background. The $\pi\text{--}\pi$ correlation lies above unity for low values of k^* , due to the enhancement stemming from Bose–Einstein quantum statistics, dominating the interaction. The repulsive Coulomb interaction has a visible impact on the correlation near $k^* = 0$ and forces $C(k^*)$ to deplete, where it finally overcomes the Bose–Einstein quantum statistics. The same behavior is observed in the correlations of $\pi\text{--}\pi$ pairs obtained from the HM dataset. An example of correlations for the k_T interval (0.70–0.90) GeV/ c for HM events is shown in Fig. 3. All correlations of the HM dataset are shown in the appendix in Fig. A.4. As for the MB results, the fits for the assumption of a polynomial of first (second) degree are shown on the left (right) panel. With increasing k_T , the onset of the $C(k^*)$ shifts systematically to higher k^* . This behavior is difficult to capture in the currently employed fitting procedure, and therefore may motivate the development of a more refined model for the correlation functions. However, it is also already known that in the case of $\pi\text{--}\pi$ correlations the fit quality improves if a 3D analysis is conducted [27, 41]. Nevertheless, the overall shapes of the $\pi\text{--}\pi$ correlations are captured by the fits in all studied m_T ranges.

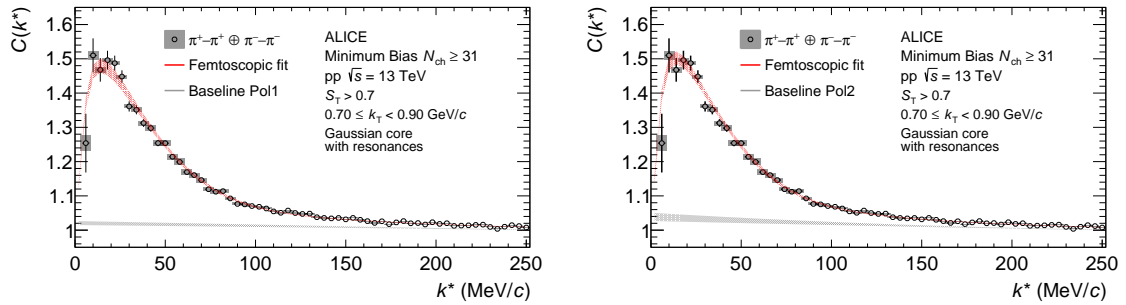


Figure 2: Correlation function of $\pi\text{--}\pi$ pairs in the third (0.50–0.70 GeV/ c) k_T interval for $N_{\text{ch}} > 30$, the fits are performed using CATS [31] employing the RSM. The left (right) panel shows the results assuming a polynomial of first (second) degree as background. The statistical and systematic uncertainties are represented by the bars and rectangles, respectively. The uncertainty bands of the fit function are obtained by employing a bootstrap [40] procedure.

The resulting $C(k^*)$ for same-sign K–p pairs in HM events are shown in Fig. 4. The correlation function lies below unity for low values of k^* indicating an overall repulsive interaction. The specific shape of the K–p correlation is the result of the interplay between the repulsive Coulomb and strong interactions.

In Figure 5, the results of the Gaussian core radius r_{core} for $\pi\text{--}\pi$ and K–p pairs in HM pp collisions at $\sqrt{s} = 13$ TeV are shown as a function of m_T together with the radii obtained from p–p correlations [6]. The agreement of the meson–meson and meson–baryon r_{core} with the m_T scaling (green band) of the p–p correlations is remarkable and provides additional support for the scenario of a common emitting source for all hadrons in small systems. Furthermore, the results presented in Fig. 6 for the three multiplicity intervals considered for MB pp collisions at $\sqrt{s} = 13$ TeV exhibit the intuitive behavior of growing r_{core} with increasing multiplicity and also show the scaling of r_{core} with increasing m_T . The degree of consistency between the data and the model is estimated by using the $\chi^2 = \sum_i (x_{\text{Data}}^i - x_{\text{Theory}}^i)^2 / (\sigma_{\text{Data}}^i)^2$ normalized to the number of degrees of freedom (NDF), commonly called the reduced χ^2 . The bot-

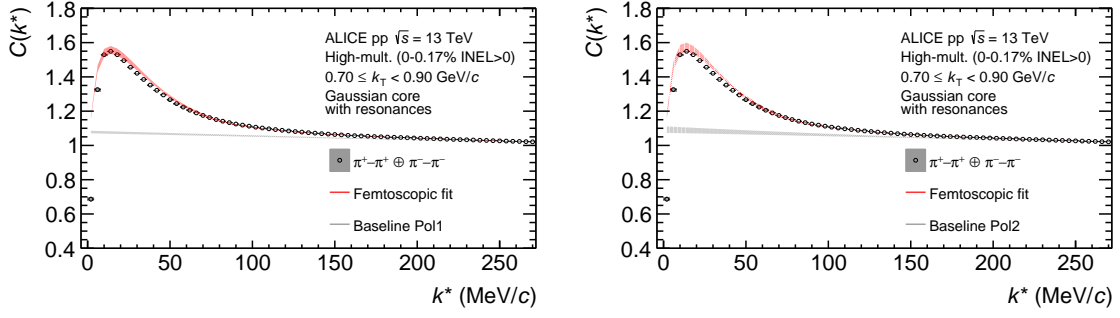


Figure 3: Correlation function of π - π pairs in the fourth (0.70 – 0.90 GeV/c) k_T interval for HM collisions, the fits on the left (right) are performed using CATS [31] employing the RSM and assuming a polynomial of first (second) degree as background. The statistical and systematic uncertainties are represented by the bars and rectangles, respectively. The uncertainty bands of the fit function are obtained by employing a bootstrap [40] procedure.

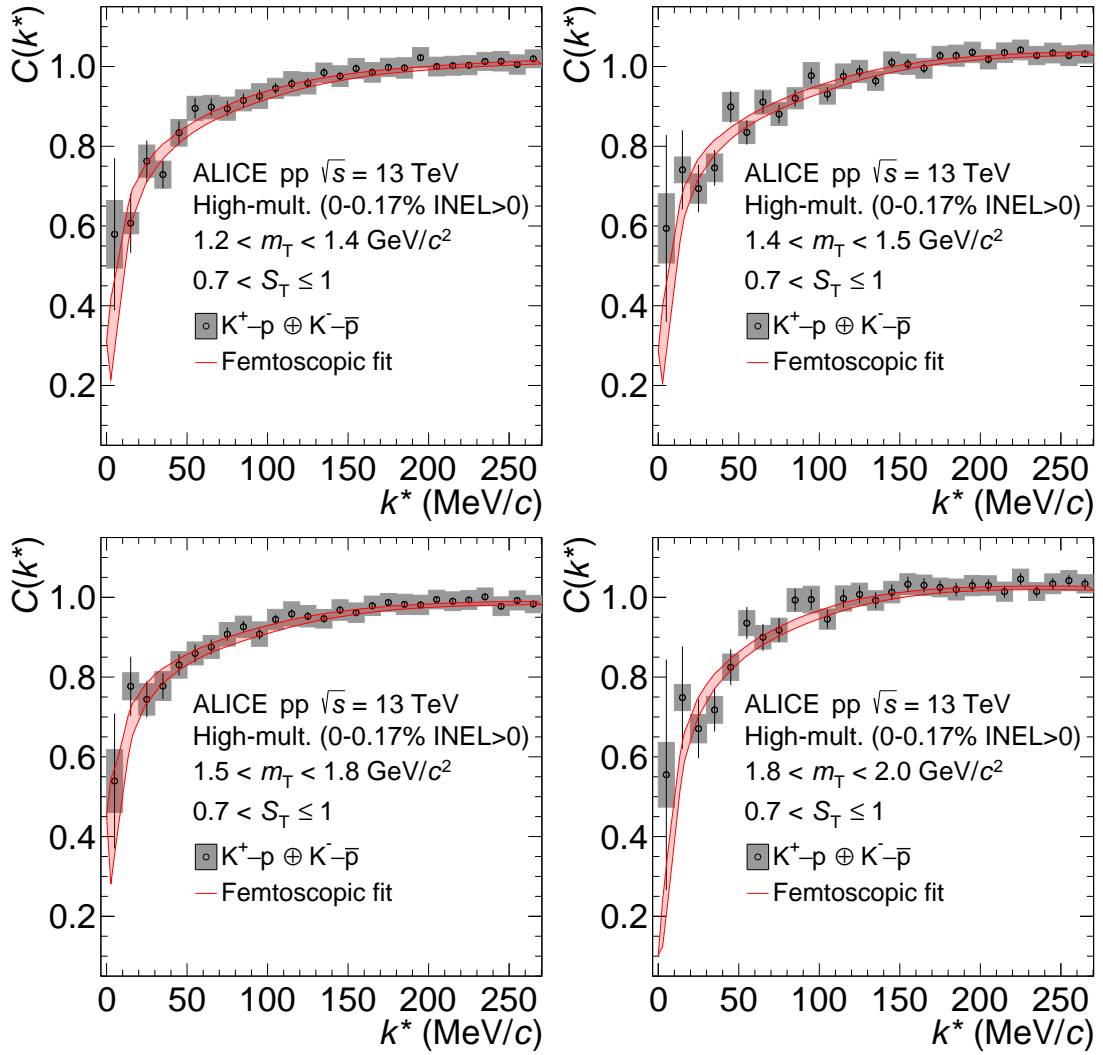


Figure 4: Correlation functions of K - p pairs in different ranges of m_T for HM pp collisions as indicated in each panel. Vertical bars represent statistical uncertainties while boxes systematic uncertainties, respectively. The fits are performed using CATS [31] employing the root mean square deviation for a uniform distribution in each k^* interval. The uncertainty bands of the fit function are obtained by employing a bootstrap [40] procedure.

tom panels in Fig. 6 show the reduced χ^2 for $6 < k^* < 100$ MeV/c, indicating that the assumption of a polynomial of second degree always performs as good or better than the first degree choice. In all the multiplicity intervals, for m_T below 0.6 GeV/c², which is probed with the π - π correlations, the r_{core} reaches a “saturation” regime and becomes independent of m_T . For K-p pairs no breaking of the m_T scaling is observed, however, it should be noted that the lowest m_T range accessed for K-p correlations in this analysis is 1.2 – 1.4 GeV/c² while the theoretical lower limit is at 0.7 GeV/c², leaving some narrow phase-space for a possible violation of the m_T scaling. A similar change in trend was already observed by CMS [33] and ALICE [27] in pp collisions at $\sqrt{s} = 13$ TeV and 900 GeV. A possible explanation for the observed trend could be related to the fact that for low- m_T pairs in pp collisions, the region of homogeneity (r_{core}) spans the entire physical extension of the hadronization hypersurface which, hence, represents the observed upper boundary of r_{core} . Any more detailed explanation will most likely require a consistent hydrodynamical treatment of small systems and a careful study of the properties of the resulting hadronization hypersurface and, hence, is outside the scope of this paper. However, these data provide valuable input for transport models which should describe the spatial extension of the particle emitting source in small systems and may inspire new theoretical works towards the description of the observed r_{core} scaling with m_T for all the measured particle pairs.

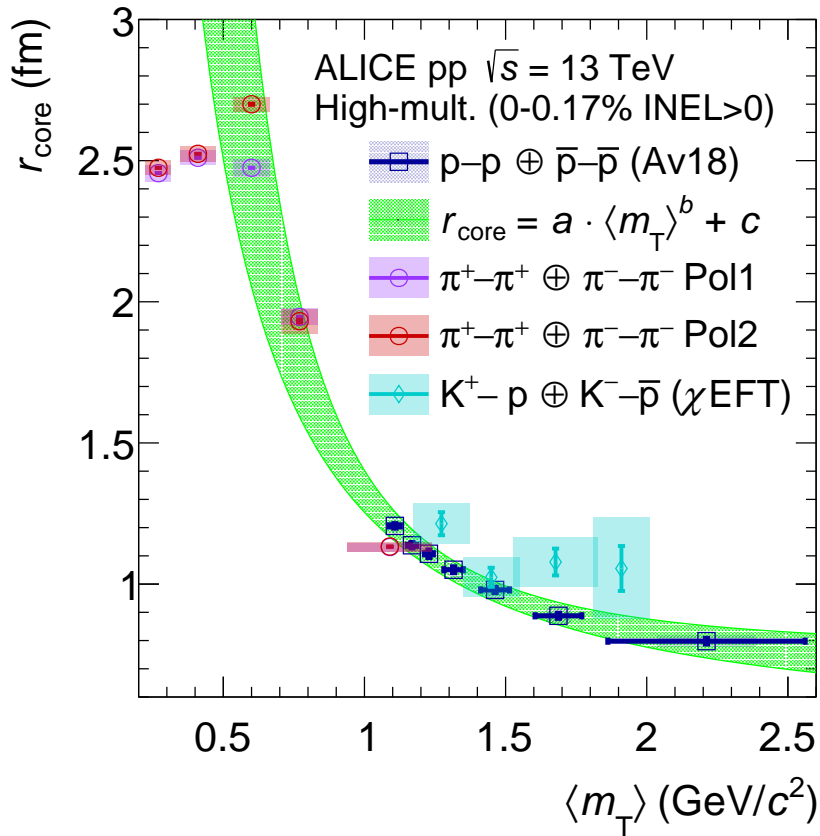


Figure 5: Extracted radii from the fit as a function of m_T for the HM analysis of meson–meson, meson–baryon (this work), and baryon–baryon [6] correlations. The green band corresponds to the parametrization of the m_T scaling of the p–p correlations and is shown with the associated 3σ spread.

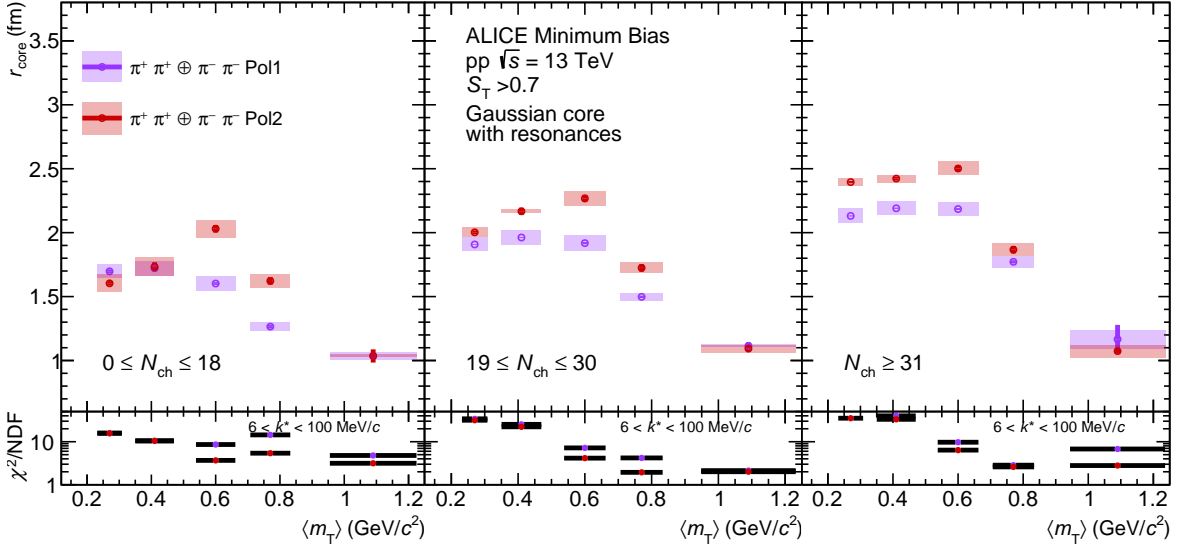


Figure 6: Extracted radii from the fits of π - π correlations as a function of m_T for three different multiplicity classes. From left to right and bottom: $1 \leq N_{\text{ch}} \leq 18$, $19 \leq N_{\text{ch}} \leq 30$ and $N_{\text{ch}} \geq 31$. The reduced χ^2 for the obtained radii is shown in the lower panels and evaluated in the range of $6 < k^* < 100$ MeV/c. The assumption that a second-order polynomial background shape exhibits either greater or equivalent compatibility with the data compared to a first-order polynomial.

6 Summary

In this work, the spatial extension of the particle source function is studied using correlations of the relative momentum of particles, referred to as femtoscopy. The source function is described by a Gaussian core and an exponential resonance halo [6]. The resonance abundances are fixed from estimations obtained within the canonical statistical hadronization model and the specific decay kinematics from the EPOS [9] event generator. This prescription allows for the first time a quantitative description of the exponential type source for π - π correlation functions in intervals of m_T . The correlation functions are studied for high multiplicity pp collisions and in multiplicity intervals for minimum bias collisions. The model is able to capture the widths of the studied correlation functions, however, cannot provide a full description of the correlation strength observed in the data for all studied multiplicity intervals, m_T ranges, and particle pairings. Further refinements of the employed model include an extension to a 3D analysis and the application of recently developed particle emission models such as CECA [15], which for now was only tested for baryon-baryon correlations. Finally, by also analyzing the K-p correlation functions in intervals of m_T within the same framework, the Gaussian core radii r_{core} are obtained and their dependence on m_T is studied. A m_T scaling for r_{core} consistent with the one reported in [6], obtained from the analysis of baryon-baryon correlations, is found for $m_T > 0.6$ GeV/c² and, hence, points to a common emitting source for all hadrons in small systems at the LHC. For $m_T < 0.6$ GeV/c², which is accessible by the π - π correlation functions a saturation of r_{core} is observed leading to a breaking of the m_T scaling. A possible explanation could be that r_{core} spans the entire physical extension of the hadronization hypersurface and hence can grow no further.

Acknowledgements

The ALICE Collaboration would like to thank all its engineers and technicians for their invaluable contributions to the construction of the experiment and the CERN accelerator teams for the outstanding

performance of the LHC complex. The ALICE Collaboration gratefully acknowledges the resources and support provided by all Grid centres and the Worldwide LHC Computing Grid (WLCG) collaboration. The ALICE Collaboration acknowledges the following funding agencies for their support in building and running the ALICE detector: A. I. Alikhanyan National Science Laboratory (Yerevan Physics Institute) Foundation (ANSL), State Committee of Science and World Federation of Scientists (WFS), Armenia; Austrian Academy of Sciences, Austrian Science Fund (FWF): [M 2467-N36] and Nationalstiftung für Forschung, Technologie und Entwicklung, Austria; Ministry of Communications and High Technologies, National Nuclear Research Center, Azerbaijan; Conselho Nacional de Desenvolvimento Científico e Tecnológico (CNPq), Financiadora de Estudos e Projetos (Finep), Fundação de Amparo à Pesquisa do Estado de São Paulo (FAPESP) and Universidade Federal do Rio Grande do Sul (UFRGS), Brazil; Bulgarian Ministry of Education and Science, within the National Roadmap for Research Infrastructures 2020-2027 (object CERN), Bulgaria; Ministry of Education of China (MOEC), Ministry of Science & Technology of China (MSTC) and National Natural Science Foundation of China (NSFC), China; Ministry of Science and Education and Croatian Science Foundation, Croatia; Centro de Aplicaciones Tecnológicas y Desarrollo Nuclear (CEADEN), Cubaenergía, Cuba; Ministry of Education, Youth and Sports of the Czech Republic, Czech Republic; The Danish Council for Independent Research | Natural Sciences, the VILLUM FONDEN and Danish National Research Foundation (DNRF), Denmark; Helsinki Institute of Physics (HIP), Finland; Commissariat à l’Energie Atomique (CEA) and Institut National de Physique Nucléaire et de Physique des Particules (IN2P3) and Centre National de la Recherche Scientifique (CNRS), France; Bundesministerium für Bildung und Forschung (BMBF) and GSI Helmholtzzentrum für Schwerionenforschung GmbH, Germany; General Secretariat for Research and Technology, Ministry of Education, Research and Religions, Greece; National Research, Development and Innovation Office, Hungary; Department of Atomic Energy Government of India (DAE), Department of Science and Technology, Government of India (DST), University Grants Commission, Government of India (UGC) and Council of Scientific and Industrial Research (CSIR), India; National Research and Innovation Agency - BRIN, Indonesia; Istituto Nazionale di Fisica Nucleare (INFN), Italy; Japanese Ministry of Education, Culture, Sports, Science and Technology (MEXT) and Japan Society for the Promotion of Science (JSPS) KAKENHI, Japan; Consejo Nacional de Ciencia (CONACYT) y Tecnología, through Fondo de Cooperación Internacional en Ciencia y Tecnología (FONCICYT) and Dirección General de Asuntos del Personal Académico (DGAPA), Mexico; Nederlandse Organisatie voor Wetenschappelijk Onderzoek (NWO), Netherlands; The Research Council of Norway, Norway; Commission on Science and Technology for Sustainable Development in the South (COMSATS), Pakistan; Pontificia Universidad Católica del Perú, Peru; Ministry of Education and Science, National Science Centre and WUT ID-UB, Poland; Korea Institute of Science and Technology Information and National Research Foundation of Korea (NRF), Republic of Korea; Ministry of Education and Scientific Research, Institute of Atomic Physics, Ministry of Research and Innovation and Institute of Atomic Physics and Universitatea Nationala de Stiinta si Tehnologie Politehnica Bucuresti, Romania; Ministry of Education, Science, Research and Sport of the Slovak Republic, Slovakia; National Research Foundation of South Africa, South Africa; Swedish Research Council (VR) and Knut & Alice Wallenberg Foundation (KAW), Sweden; European Organization for Nuclear Research, Switzerland; Suranaree University of Technology (SUT), National Science and Technology Development Agency (NSTDA) and National Science, Research and Innovation Fund (NSRF via PMU-B B05F650021), Thailand; Turkish Energy, Nuclear and Mineral Research Agency (TENMAK), Turkey; National Academy of Sciences of Ukraine, Ukraine; Science and Technology Facilities Council (STFC), United Kingdom; National Science Foundation of the United States of America (NSF) and United States Department of Energy, Office of Nuclear Physics (DOE NP), United States of America. In addition, individual groups or members have received support from: Czech Science Foundation (grant no. 23-07499S), Czech Republic; European Research Council, Strong 2020 - Horizon 2020 (grant nos. 950692, 824093), European Union; ICSC - Centro Nazionale di Ricerca in High Performance Computing, Big Data and Quantum Computing, European Union - NextGenerationEU; Academy of Finland (Center of Excellence in Quark Matter) (grant nos.

346327, 346328), Finland.

References

- [1] M. A. Lisa, S. Pratt, R. Soltz, and U. Wiedemann, “Femtoscopy in relativistic heavy ion collisions”, *Ann. Rev. Nucl. Part. Sci.* **55** (2005) 357–402, arXiv:nuc1-ex/0505014 [nucl-ex].
- [2] L. Fabbietti, V. Mantovani Sarti, and O. Vazquez Doce, “Study of the Strong Interaction Among Hadrons with Correlations at the LHC”, *Ann. Rev. Nucl. Part. Sci.* **71** (2021) 377–402, arXiv:2012.09806 [nucl-ex].
- [3] M. Chojnacki, A. Kisiel, W. Florkowski, and W. Broniowski, “Therminator 2: Thermal heavy ion generator 2”, *Computer Physics Communications* **183** (2012) 746–773.
<https://www.sciencedirect.com/science/article/pii/S0010465511003808>.
- [4] A. Kisiel, M. Gałazyn, and P. Bożek, “Pion, kaon, and proton femtoscopy in pb-pb collisions at $\sqrt{s_{NN}} = 2.76$ tev modeled in (3+1)d hydrodynamics”, *Phys. Rev. C* **90** (Dec, 2014) 064914.
<https://link.aps.org/doi/10.1103/PhysRevC.90.064914>.
- [5] V. Shapoval, P. Braun-Munzinger, I. Karpenko, and Y. Sinyukov, “Femtoscopy correlations of kaons in pb+pb collisions at lhc within hydrokinetic model”, *Nuclear Physics A* **929** (2014) 1–8.
<https://www.sciencedirect.com/science/article/pii/S0375947414001183>.
- [6] ALICE Collaboration, S. Acharya *et al.*, “Search for a common baryon source in high-multiplicity pp collisions at the LHC”, *Phys. Lett. B* **811** (2020) 135849, arXiv:2004.08018 [nucl-ex]. [Corrigendum: *Phys. Lett. B* 861 (2025) 139233].
- [7] ALICE Collaboration, K. Aamodt *et al.*, “The ALICE experiment – A journey through QCD”, arXiv:2211.04384 [nucl-ex].
- [8] A. Andronic, P. Braun-Munzinger, K. Redlich, and J. Stachel, “Decoding the phase structure of QCD via particle production at high energy”, *Nature* **561** (2018) 321–330, arXiv:1710.09425 [nucl-th].
- [9] T. Pierog, I. Karpenko, J. M. Katzy, E. Yatsenko, and K. Werner, “EPOS LHC: Test of collective hadronization with data measured at the CERN Large Hadron Collider”, *Phys. Rev. C* **92** (2015) 034906.
- [10] ALICE Collaboration, S. Acharya *et al.*, “Unveiling the strong interaction among hadrons at the LHC”, *Nature* **588** (2020) 232–238, arXiv:2005.11495 [nucl-ex]. [Erratum: *Nature* ibid 590, E13 (2021)].
- [11] ALICE Collaboration, S. Acharya *et al.*, “Scattering Studies with Low-Energy Kaon-Proton Femtoscopy in Proton-Proton Collisions at the LHC”, *Phys. Rev. Lett.* **124** (Mar, 2020) 092301.
<https://link.aps.org/doi/10.1103/PhysRevLett.124.092301>.
- [12] ALICE Collaboration, S. Acharya *et al.*, “Exploring the $N\Lambda$ – $N\Sigma$ coupled system with high precision correlation techniques at the LHC”, *Phys. Lett. B* **833** (2022) 137272, arXiv:2104.04427 [nucl-ex].
- [13] ALICE Collaboration, S. Acharya *et al.*, “First measurement of the Λ – Ξ interaction in proton-proton collisions at the LHC”, *Phys. Lett. B* **844** (2023) 137223, arXiv:2204.10258 [nucl-ex].

- [14] ALICE Collaboration, S. Acharya *et al.*, “Experimental Evidence for an Attractive p - ϕ Interaction”, *Phys. Rev. Lett.* **127** (2021) 172301, arXiv:2105.05578 [nucl-ex].
- [15] D. Mihaylov and J. González González, “Novel model for particle emission in small collision systems”, *Eur. Phys. J. C* **83** (2023) 590, arXiv:2305.08441 [hep-ph].
- [16] T. Sjöstrand *et al.*, “An Introduction to PYTHIA 8.2”, *Comput. Phys. Commun.* **191** (2015) 159–177.
- [17] ALICE Collaboration, K. Aamodt *et al.*, “The ALICE experiment at the CERN LHC”, *Journal of Instrumentation* **3** (2008) S08002. <http://stacks.iop.org/1748-0221/3/i=08/a=S08002>.
- [18] ALICE Collaboration, B. Abelev *et al.*, “Performance of the ALICE experiment at the CERN LHC”, *Int. J. Mod. Phys. A* **29** (2014) 1430044, arXiv:1402.4476 [nucl-ex].
- [19] ALICE Collaboration, E. Abbas *et al.*, “Performance of the ALICE VZERO system”, *JINST* **8** (2013) P10016, arXiv:1306.3130 [nucl-ex].
- [20] ALICE Collaboration, K. Aamodt *et al.*, “Alignment of the ALICE Inner Tracking System with cosmic-ray tracks”, *JINST* **5** (2010) P03003, arXiv:1001.0502 [physics.ins-det].
- [21] J. Alme, Y. Andres, H. Appelshäuser, S. Bablok, N. Bialas, *et al.*, “The ALICE TPC, a large 3-dimensional tracking device with fast readout for ultra-high multiplicity events”, *Nucl.Instrum.Meth. A* **622** (2010) 316–367, arXiv:1001.1950 [physics.ins-det].
- [22] A. Akindinov *et al.*, “Performance of the ALICE Time-Of-Flight detector at the LHC”, *Eur. Phys. J. Plus* **128** (2013) 44.
- [23] ALICE Collaboration, S. Acharya *et al.*, “Constraining the $\bar{K}N$ coupled channel dynamics using femtoscopic correlations at the LHC”, *Eur. Phys. J. C* **83** (2023) 340, arXiv:2205.15176 [nucl-ex].
- [24] ALICE Collaboration, B. Abelev *et al.*, “Transverse sphericity of primary charged particles in minimum bias proton-proton collisions at $\sqrt{s} = 0.9, 2.76$ and 7 TeV”, *Eur. Phys. J. C* **72** (2012) 2124, arXiv:1205.3963 [hep-ex].
- [25] ALICE Collaboration, S. Acharya *et al.*, “Event-shape and multiplicity dependence of freeze-out radii in pp collisions at $\sqrt{s} = 7$ TeV”, *JHEP* **09** (2019) 108, arXiv:1901.05518 [nucl-ex].
- [26] ALICE Collaboration, S. Acharya *et al.*, “Accessing the strong interaction between Λ baryons and charged kaons with the femtoscopy technique at the LHC”, *Phys. Lett. B* **845** (2023) 138145, arXiv:2305.19093 [nucl-ex].
- [27] ALICE Collaboration, K. Aamodt *et al.*, “Femtoscopy of pp collisions at $\sqrt{s} = 0.9$ and 7 TeV at the LHC with two-pion Bose-Einstein correlations”, *Phys. Rev. D* **84** (2011) 112004, arXiv:1101.3665 [hep-ex].
- [28] ALICE Collaboration, S. Acharya *et al.*, “Investigating the role of strangeness in baryon–antibaryon annihilation at the LHC”, *Phys. Lett. B* **829** (2022) 137060, arXiv:2105.05190 [nucl-ex].
- [29] ALICE Collaboration, J. Adam *et al.*, “One-dimensional pion, kaon, and proton femtoscopy in Pb-Pb collisions at $\sqrt{s_{NN}} = 2.76$ TeV”, *Phys. Rev. C* **92** (2015) 054908, arXiv:1506.07884 [nucl-ex].

- [30] R. Brun, F. Bruyant, M. Maire, A. C. McPherson, and P. Zancarini, *GEANT 3: user's guide Geant 3.10, Geant 3.11; rev. version*. CERN, Geneva, 1987. <https://cds.cern.ch/record/1119728>.
- [31] D. L. Mihaylov, V. Mantovani Sarti, O. W. Arnold, L. Fabbietti, B. Hohlweger, and A. M. Mathis, “A femtoscopic correlation analysis tool using the Schrödinger equation (CATS)”, *The European Physical Journal C* **78** (2018) 394. <https://doi.org/10.1140/epjc/s10052-018-5859-0>.
- [32] K. Aoki and D. Jido, “KN scattering amplitude revisited in a chiral unitary approach and a possible broad resonance in $S = +1$ channel”, *PTEP* **2019** (2019) 013D01, arXiv:1806.00925 [nucl-th].
- [33] CMS Collaboration, A. M. Sirunyan *et al.*, “Bose-Einstein correlations of charged hadrons in proton-proton collisions at $\sqrt{s} = 13$ TeV”, *JHEP* **03** (2020) 014, arXiv:1910.08815 [hep-ex].
- [34] ATLAS Collaboration, G. Aad *et al.*, “Two-particle Bose–Einstein correlations in pp collisions at $\sqrt{s}=0.9$ and 7 TeV measured with the ATLAS detector”, *Eur. Phys. J. C* **75** (2015) 466, arXiv:1502.07947 [hep-ex].
- [35] ALICE Collaboration, S. Acharya *et al.*, “p-p, p- Λ and Λ - Λ correlations studied via femtoscopy in pp reactions at $\sqrt{s} = 7$ TeV”, *Phys. Rev. C* **99** (2019) 024001, arXiv:1805.12455 [nucl-ex].
- [36] CMS Collaboration, A. M. Sirunyan *et al.*, “Bose-Einstein correlations in pp, pPb, and PbPb collisions at $\sqrt{s_{NN}} = 0.9$ –7 TeV”, *Phys. Rev. C* **97** (2018) 064912, arXiv:1712.07198 [hep-ex].
- [37] C. T. H. S., and W. Zajc, “Bose-Einstein correlations for Lévy stable source distributions.”, *Eur. Phys. J. C* **36** (2004) 67–78.
- [38] V. Vovchenko and H. Stoecker, “Thermal-FIST: A package for heavy-ion collisions and hadronic equation of state”, *Comput. Phys. Commun.* **244** (2019) 295–310, arXiv:1901.05249 [nucl-th].
- [39] V. Vovchenko, B. Dönigus, and H. Stoecker, “Canonical statistical model analysis of p-p, p-Pb, and Pb-Pb collisions at energies available at the CERN Large Hadron Collider”, *Phys. Rev. C* **100** (2019) 054906, arXiv:1906.03145 [hep-ph].
- [40] W. H. Press, S. A. Teukolsky, W. T. Vetterling, and B. P. Flannery, *Numerical Recipes 3rd Edition: The Art of Scientific Computing*. Cambridge University Press, 2007.
- [41] ALICE Collaboration, J. Adam *et al.*, “Two-pion femtoscopy in p-Pb collisions at $\sqrt{s_{NN}} = 5.02$ TeV”, *Phys. Rev. C* **91** (2015) 034906, arXiv:1502.00559 [nucl-ex].

A Same Charge Pion Correlation Functions

Correlation functions of same-sign π - π pairs in bins of k_T are shown in Figs. A.1, A.2, and A.3 for the three multiplicity classes of MB collisions and in Fig A.4 for the HM dataset. The systematic uncertainties are represented by boxes. The fits performed using CATS [31] employing the RSM are also displayed in the figures for the different k_T and multiplicity classes. The uncertainty bands of the fit function are obtained by employing a bootstrap [40] procedure. The left (right) panels of the Figures show the results assuming a polynomial of first (second) degree to describe the baseline of the $C(k^*)$.

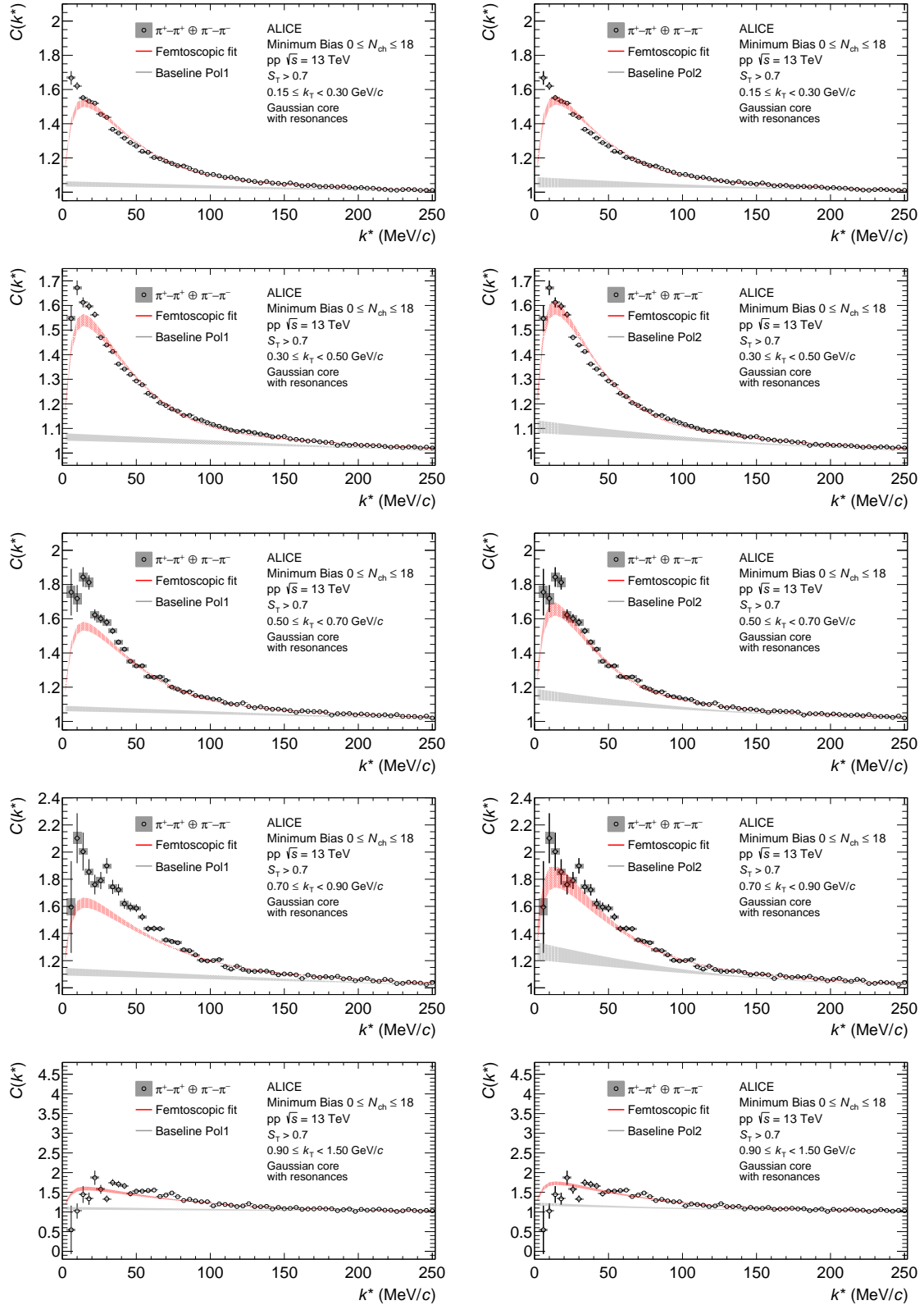


Figure A.1: Correlation functions of π - π pairs in bins of k_T for $1 \leq N_{\text{ch}} \leq 18$, the fits are performed using CATS [31] employing the RSM. The left (right) panels show the results assuming a polynomial of first (second) degree as background. The uncertainties of the data points are obtained by varying the selection criteria as described in the text. The uncertainty bands of the fit function are obtained by employing a bootstrap [40] procedure.

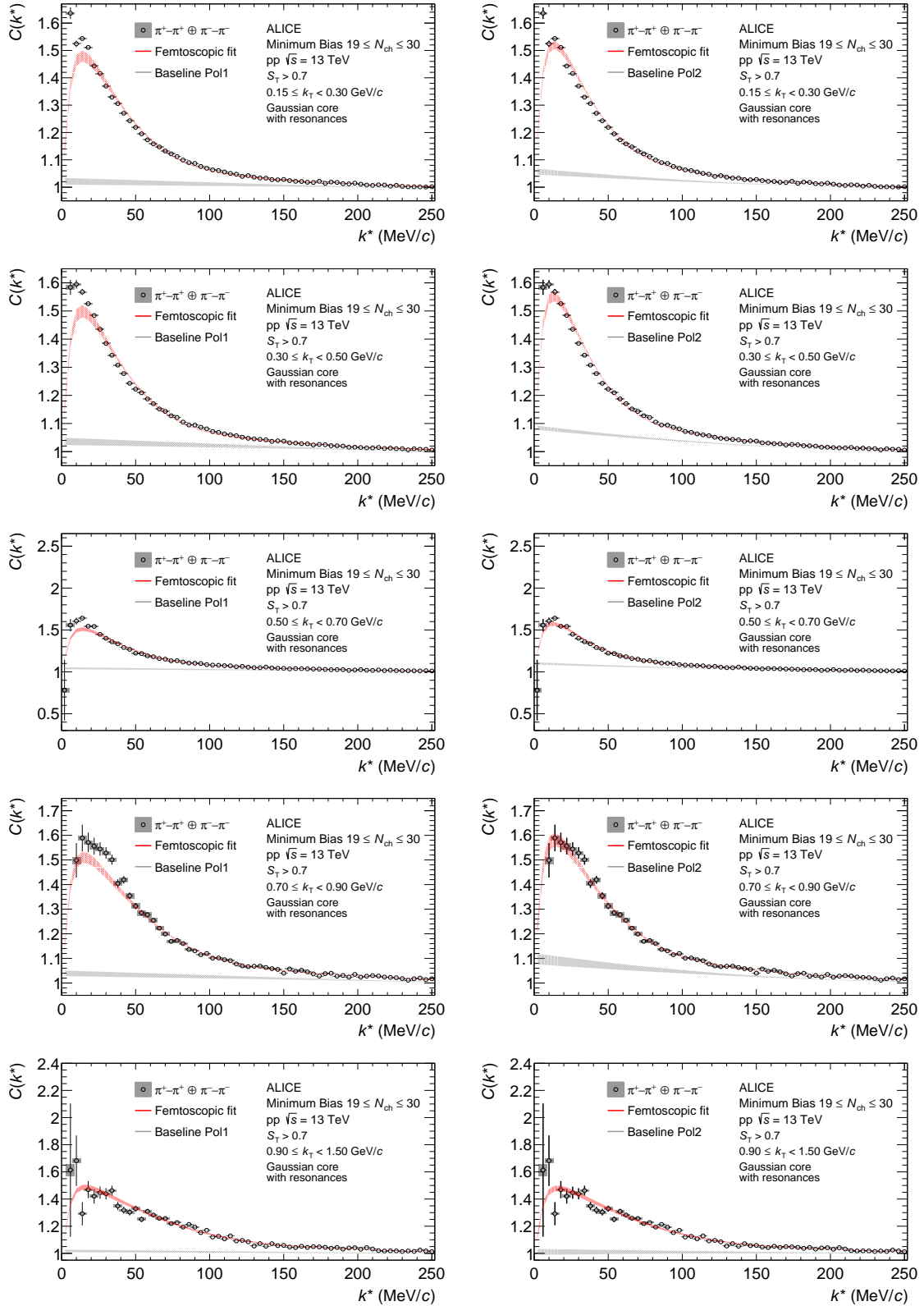


Figure A.2: Correlation functions of π - π pairs in bins of k_T for $19 \leq N_{\text{ch}} \leq 30$, the fits are performed using CATS [31] employing the RSM. The left (right) panels show the results assuming a polynomial of first (second) degree as background. The uncertainties of the data points are obtained by varying the selection criteria as described in the text. The uncertainty bands of the fit function are obtained by employing a bootstrap [40] procedure.

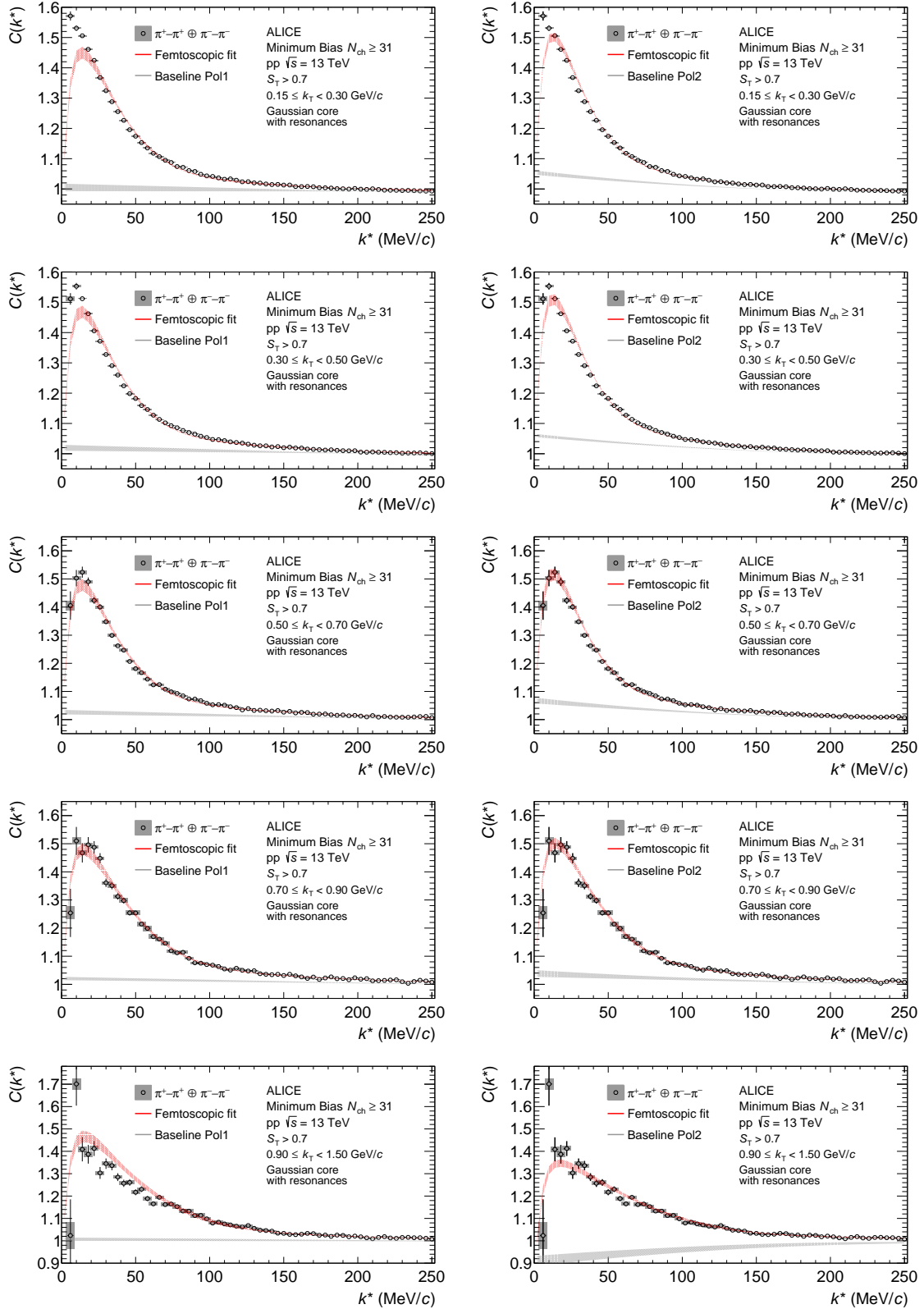


Figure A.3: Correlation functions of π - π pairs in bins of k_T for $N_{\text{ch}} \geq 31$, the fits are performed using CATS [31] employing the RSM. The left (right) panels show the results assuming a polynomial of first (second) degree as background. The uncertainties of the data points are obtained by varying the selection criteria as described in the text. The uncertainty bands of the fit function are obtained by employing a bootstrap [40] procedure.

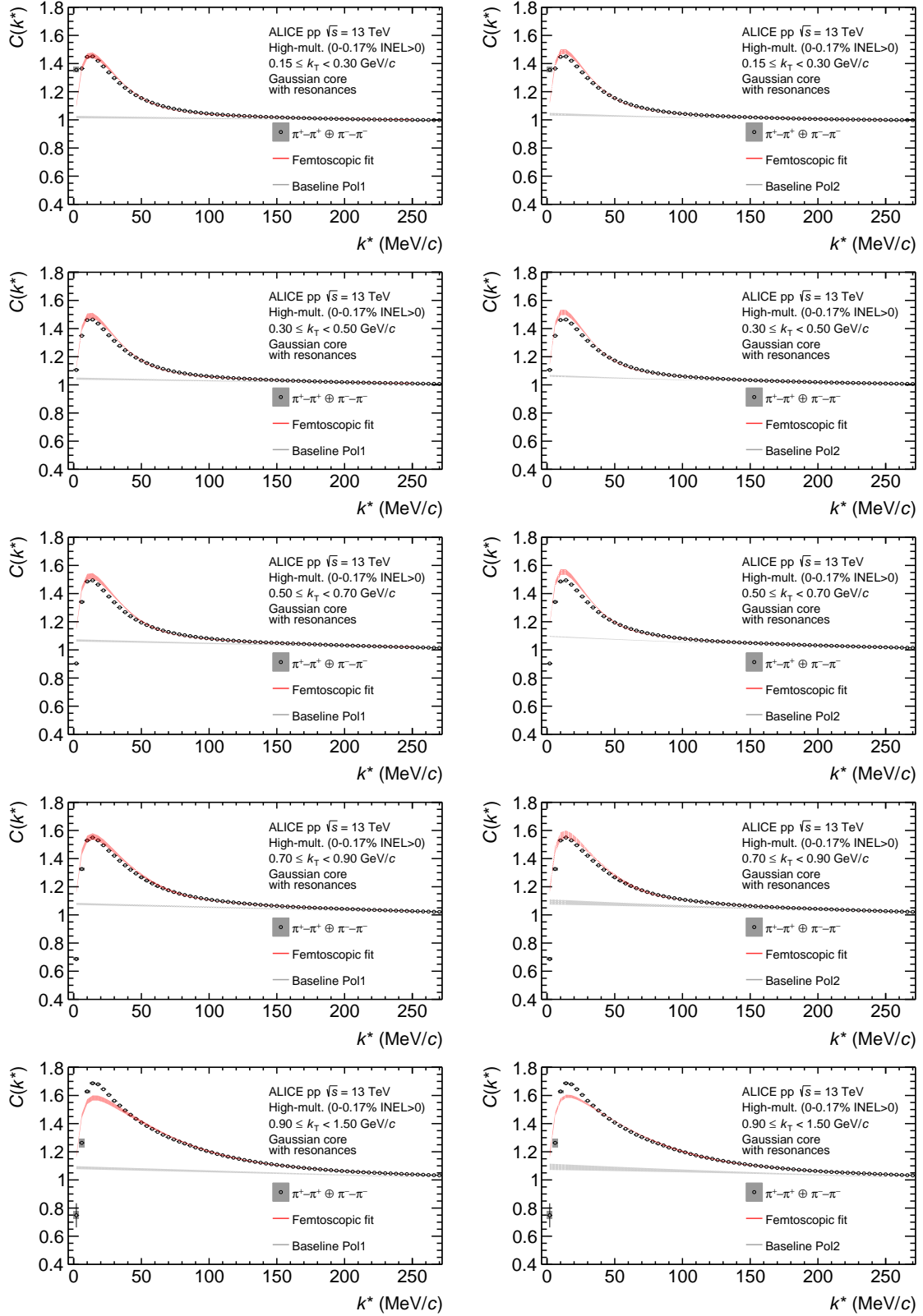


Figure A.4: Correlation functions of π - π in bins of k_T for HM collisions, the fits on the left (right) are performed using CATS [31] employing the RSM and assuming a polynomial of first (second) degree as background. The uncertainties of the data points are obtained by varying the selection criteria as described in the text. The uncertainty bands of the fit function are obtained by employing a bootstrap [40] procedure.

B The ALICE Collaboration

S. Acharya ¹²⁸, D. Adamová ⁸⁷, G. Aglieri Rinella ³³, M. Agnello ³⁰, N. Agrawal ⁵², Z. Ahammed ¹³⁶, S. Ahmad ¹⁶, S.U. Ahn ⁷², I. Ahuja ³⁸, A. Akhmedov ¹⁴², M. Al-Turany ⁹⁸, D. Aleksandrov ¹⁴², B. Alessandro ⁵⁷, H.M. Alfanda ⁶, R. Alfaro Molina ⁶⁸, B. Ali ¹⁶, A. Alici ²⁶, N. Alizadehvandchali ¹¹⁷, A. Alkin ³³, J. Alme ²¹, G. Alocco ⁵³, T. Alt ⁶⁵, A.R. Altamura ⁵¹, I. Altsybeev ⁹⁶, J.R. Alvarado ⁴⁵, M.N. Anaam ⁶, C. Andrei ⁴⁶, N. Andreou ¹¹⁶, A. Andronic ¹²⁷, E. Andronov ¹⁴², V. Anguelov ⁹⁵, F. Antinori ⁵⁵, P. Antonioli ⁵², N. Apadula ⁷⁵, L. Aphecetche ¹⁰⁴, H. Appelshäuser ⁶⁵, C. Arata ⁷⁴, S. Arcelli ²⁶, M. Aresti ²³, R. Arnaldi ⁵⁷, J.G.M.C.A. Arneiro ¹¹¹, I.C. Arsene ²⁰, M. Arslandok ¹³⁹, A. Augustinus ³³, R. Averbeck ⁹⁸, M.D. Azmi ¹⁶, H. Baba ¹²⁵, A. Badalà ⁵⁴, J. Bae ¹⁰⁵, Y.W. Baek ⁴¹, X. Bai ¹²¹, R. Bailhache ⁶⁵, Y. Bailung ⁴⁹, R. Bala ⁹², A. Balbino ³⁰, A. Baldisseri ¹³¹, B. Balis ², D. Banerjee ⁴, Z. Banoo ⁹², F. Barile ³², L. Barioglio ⁹⁶, M. Barlou ⁷⁹, B. Barman ⁴², G.G. Barnaföldi ⁴⁷, L.S. Barnby ⁸⁶, E. Barreau ¹⁰⁴, V. Barret ¹²⁸, L. Barreto ¹¹¹, C. Bartels ¹²⁰, K. Barth ³³, E. Bartsch ⁶⁵, N. Bastid ¹²⁸, S. Basu ^{1,76}, G. Batigne ¹⁰⁴, D. Battistini ⁹⁶, B. Batyunya ¹⁴³, D. Bauri ⁴⁸, J.L. Bazo Alba ¹⁰², I.G. Bearden ⁸⁴, C. Beattie ¹³⁹, P. Becht ⁹⁸, D. Behera ⁴⁹, I. Belikov ¹³⁰, A.D.C. Bell Hechavarria ¹²⁷, F. Bellini ²⁶, R. Bellwied ¹¹⁷, S. Belokurova ¹⁴², L.G.E. Beltran ¹¹⁰, Y.A.V. Beltran ⁴⁵, G. Bencedi ⁴⁷, S. Beole ²⁵, Y. Berdnikov ¹⁴², A. Berdnikova ⁹⁵, L. Bergmann ⁹⁵, M.G. Besoiu ⁶⁴, L. Betev ³³, P.P. Bhaduri ¹³⁶, A. Bhasin ⁹², M.A. Bhat ⁴, B. Bhattacharjee ⁴², L. Bianchi ²⁵, N. Bianchi ⁵⁰, J. Bielčik ³⁶, J. Bielčíková ⁸⁷, A.P. Bigot ¹³⁰, A. Bilandzic ⁹⁶, G. Biro ⁴⁷, S. Biswas ⁴, N. Bize ¹⁰⁴, J.T. Blair ¹⁰⁹, D. Blau ¹⁴², M.B. Blidaru ⁹⁸, N. Bluhme ³⁹, C. Blume ⁶⁵, G. Boca ^{22,56}, F. Bock ⁸⁸, T. Bodova ²¹, S. Boi ²³, J. Bok ¹⁷, L. Boldizsár ⁴⁷, M. Bombara ³⁸, P.M. Bond ³³, G. Bonomi ^{135,56}, H. Borel ¹³¹, A. Borissov ¹⁴², A.G. Borquez Carcamo ⁹⁵, H. Bossi ¹³⁹, E. Botta ²⁵, Y.E.M. Bouziani ⁶⁵, L. Bratrud ⁶⁵, P. Braun-Munzinger ⁹⁸, M. Bregant ¹¹¹, M. Broz ³⁶, G.E. Bruno ^{97,32}, M.D. Buckland ²⁴, D. Budnikov ¹⁴², H. Buesching ⁶⁵, S. Bufalino ³⁰, P. Buhler ¹⁰³, N. Burmasov ¹⁴², Z. Buthelezi ^{69,124}, A. Bylinkin ²¹, S.A. Bysiak ¹⁰⁸, J.C. Cabanillas Noris ¹¹⁰, M. Cai ⁶, H. Caines ¹³⁹, A. Caliva ²⁹, E. Calvo Villar ¹⁰², J.M.M. Camacho ¹¹⁰, P. Camerini ²⁴, F.D.M. Canedo ¹¹¹, S.L. Cantway ¹³⁹, M. Carabas ¹¹⁴, A.A. Carballo ³³, F. Carnesecchi ³³, R. Caron ¹²⁹, L.A.D. Carvalho ¹¹¹, J. Castillo Castellanos ¹³¹, F. Catalano ^{33,25}, C. Ceballos Sanchez ¹⁴³, I. Chakaberia ⁷⁵, P. Chakraborty ⁴⁸, S. Chandra ¹³⁶, S. Chapeland ³³, M. Chartier ¹²⁰, S. Chattopadhyay ¹³⁶, S. Chattopadhyay ¹⁰⁰, T. Cheng ^{98,6}, C. Cheshkov ¹²⁹, B. Cheynis ¹²⁹, V. Chibante Barroso ³³, D.D. Chinellato ¹¹², E.S. Chizzali ^{17,96}, J. Cho ⁵⁹, S. Cho ⁵⁹, P. Chochula ³³, D. Choudhury ⁴², P. Christakoglou ⁸⁵, C.H. Christensen ⁸⁴, P. Christiansen ⁷⁶, T. Chujo ¹²⁶, M. Ciaccio ³⁰, C. Cicalo ⁵³, M.R. Ciupek ⁹⁸, G. Clai ^{III,52}, F. Colamaria ⁵¹, J.S. Colburn ¹⁰¹, D. Colella ^{97,32}, M. Colocci ²⁶, M. Concas ³³, G. Conesa Balbastre ⁷⁴, Z. Conesa del Valle ¹³², G. Contin ²⁴, J.G. Contreras ³⁶, M.L. Coquet ¹³¹, P. Cortese ^{134,57}, M.R. Cosentino ¹¹³, F. Costa ³³, S. Costanza ^{22,56}, C. Cot ¹³², J. Crkovská ⁹⁵, P. Crochet ¹²⁸, R. Cruz-Torres ⁷⁵, P. Cui ⁶, A. Dainese ⁵⁵, M.C. Danisch ⁹⁵, A. Danu ⁶⁴, P. Das ⁸¹, P. Das ⁴, S. Das ⁴, A.R. Dash ¹²⁷, S. Dash ⁴⁸, A. De Caro ²⁹, G. de Cataldo ⁵¹, J. de Cuveland ³⁹, A. De Falco ²³, D. De Gruttola ²⁹, N. De Marco ⁵⁷, C. De Martin ²⁴, S. De Pasquale ²⁹, R. Deb ¹³⁵, R. Del Grande ⁹⁶, L. Dello Stritto ^{33,29}, W. Deng ⁶, P. Dhankher ¹⁹, D. Di Bari ³², A. Di Mauro ³³, B. Diab ¹³¹, R.A. Diaz ^{143,7}, T. Dietel ¹¹⁵, Y. Ding ⁶, J. Ditzel ⁶⁵, R. Divià ³³, D.U. Dixit ¹⁹, Ø. Djuvlsland ²¹, U. Dmitrieva ¹⁴², A. Dobrin ⁶⁴, B. Dönigus ⁶⁵, J.M. Dubinski ¹³⁷, A. Dubla ⁹⁸, S. Dudi ⁹¹, P. Dupieux ¹²⁸, M. Durkac ¹⁰⁷, N. Dzalaiova ¹³, T.M. Eder ¹²⁷, R.J. Ehlers ⁷⁵, F. Eisenhut ⁶⁵, R. Ejima ⁹³, D. Elia ⁵¹, B. Erazmus ¹⁰⁴, F. Ercolessi ²⁶, B. Espagnon ¹³², G. Eulisse ³³, D. Evans ¹⁰¹, S. Evdokimov ¹⁴², L. Fabbietti ⁹⁶, M. Faggin ²⁸, J. Faivre ⁷⁴, F. Fan ⁶, W. Fan ⁷⁵, A. Fantoni ⁵⁰, M. Fasel ⁸⁸, A. Feliciello ⁵⁷, G. Feofilov ¹⁴², A. Fernández Téllez ⁴⁵, L. Ferrandi ¹¹¹, M.B. Ferrer ³³, A. Ferrero ¹³¹, C. Ferrero ^{IV,57}, A. Ferretti ²⁵, V.J.G. Feuillard ⁹⁵, V. Filova ³⁶, D. Finogeev ¹⁴², F.M. Fionda ⁵³, E. Flatland ³³, F. Flor ¹¹⁷, A.N. Flores ¹⁰⁹, S. Foertsch ⁶⁹, I. Fokin ⁹⁵, S. Fokin ¹⁴², E. Fragiaco ⁵⁸, E. Frajna ⁴⁷, U. Fuchs ³³, N. Funicello ²⁹, C. Furget ⁷⁴, A. Furs ¹⁴², T. Fusayasu ⁹⁹, J.J. Gaardhøje ⁸⁴, M. Gagliardi ²⁵, A.M. Gago ¹⁰², T. Gahlaut ⁴⁸, C.D. Galvan ¹¹⁰, D.R. Gangadharan ¹¹⁷, P. Ganoti ⁷⁹, C. Garabatos ⁹⁸, T. García Chávez ⁴⁵, E. García-Solis ⁹, C. Gargiulo ³³, P. Gasik ⁹⁸, A. Gautam ¹¹⁹, M.B. Gay Ducati ⁶⁷, M. Germain ¹⁰⁴, A. Ghimouz ¹²⁶, C. Ghosh ¹³⁶, M. Giacalone ⁵², G. Gioachin ³⁰, P. Giubellino ^{98,57}, P. Giubilato ²⁸, A.M.C. Glaenger ¹³¹, P. Glässel ⁹⁵, E. Glimos ¹²³, D.J.Q. Goh ⁷⁷, V. Gonzalez ¹³⁸, P. Gordeev ¹⁴², M. Gorgon ², K. Goswami ⁴⁹, S. Gotovac ³⁴, V. Grabski ⁶⁸, L.K. Graczykowski ¹³⁷, E. Grecka ⁸⁷, A. Grelli ⁶⁰, C. Grigoras ³³, V. Grigoriev ¹⁴², S. Grigoryan ^{143,1}, F. Grosa ³³, J.F. Grosse-Oetringhaus ³³, R. Grosso ⁹⁸, D. Grund ³⁶, N.A. Grunwald ⁹⁵, G.G. Guardiani ¹¹², R. Guernane ⁷⁴, M. Guilbaud ¹⁰⁴, K. Gulbrandsen ⁸⁴, T. Gündem ⁶⁵, T. Gunji ¹²⁵,

W. Guo ⁶, A. Gupta ⁹², R. Gupta ⁹², R. Gupta ⁴⁹, K. Gwizdziel ¹³⁷, L. Gyulai ⁴⁷, C. Hadjidakis ¹³², F.U. Haider ⁹², S. Haidlova ³⁶, M. Haldar ⁴, H. Hamagaki ⁷⁷, A. Hamdi ⁷⁵, Y. Han ¹⁴⁰, B.G. Hanley ¹³⁸, R. Hannigan ¹⁰⁹, J. Hansen ⁷⁶, J.W. Harris ¹³⁹, A. Harton ⁹, M.V. Hartung ⁶⁵, H. Hassan ¹¹⁸, D. Hatzifotiadou ⁵², P. Hauer ⁴³, L.B. Havener ¹³⁹, E. Hellbär ⁹⁸, H. Helstrup ³⁵, M. Hemmer ⁶⁵, T. Herman ³⁶, G. Herrera Corral ⁸, F. Herrmann ¹²⁷, S. Herrmann ¹²⁹, K.F. Hetland ³⁵, B. Heybeck ⁶⁵, H. Hillemanns ³³, B. Hippolyte ¹³⁰, F.W. Hoffmann ⁷¹, B. Hofman ⁶⁰, G.H. Hong ¹⁴⁰, M. Horst ⁹⁶, A. Horzyk ², Y. Hou ⁶, P. Hristov ³³, C. Hughes ¹²³, P. Huhn ⁶⁵, L.M. Huhta ¹¹⁸, T.J. Humanic ⁸⁹, A. Hutson ¹¹⁷, D. Hutter ³⁹, M.C. Hwang ¹⁹, R. Ilkaev ¹⁴², H. Ilyas ¹⁴, M. Inaba ¹²⁶, G.M. Innocenti ³³, M. Ippolitov ¹⁴², A. Isakov ^{85,87}, T. Isidori ¹¹⁹, M.S. Islam ¹⁰⁰, M. Ivanov ⁹⁸, M. Ivanov ¹³, V. Ivanov ¹⁴², K.E. Iversen ⁷⁶, M. Jablonski ², B. Jacak ^{19,75}, N. Jacazio ²⁶, P.M. Jacobs ⁷⁵, S. Jadlovská ¹⁰⁷, J. Jadlovsky ¹⁰⁷, S. Jaelani ⁸³, C. Jahnke ¹¹¹, M.J. Jakubowska ¹³⁷, M.A. Janik ¹³⁷, T. Janson ⁷¹, S. Ji ¹⁷, S. Jia ¹⁰, A.A.P. Jimenez ⁶⁶, F. Jonas ^{75,88,127}, D.M. Jones ¹²⁰, J.M. Jowett ^{33,98}, J. Jung ⁶⁵, M. Jung ⁶⁵, A. Junique ³³, A. Jusko ¹⁰¹, J. Kaewjai ¹⁰⁶, P. Kalinak ⁶¹, A.S. Kalteyer ⁹⁸, A. Kalweit ³³, A. Karasu Uysal ^{V,73}, D. Karatovic ⁹⁰, O. Karavichev ¹⁴², T. Karavicheva ¹⁴², P. Karczmarczyk ¹³⁷, E. Karpechev ¹⁴², M.J. Karwowska ^{33,137}, U. Keschull ⁷¹, R. Keidel ¹⁴¹, D.L.D. Keijdener ⁶⁰, M. Keil ³³, B. Ketzer ⁴³, S.S. Khade ⁴⁹, A.M. Khan ¹²¹, S. Khan ¹⁶, A. Khanzadeev ¹⁴², Y. Kharlov ¹⁴², A. Khatun ¹¹⁹, A. Khuntia ³⁶, Z. Khuranova ⁶⁵, B. Kileng ³⁵, B. Kim ¹⁰⁵, C. Kim ¹⁷, D.J. Kim ¹¹⁸, E.J. Kim ⁷⁰, J. Kim ¹⁴⁰, J. Kim ⁵⁹, J. Kim ⁷⁰, M. Kim ¹⁹, S. Kim ¹⁸, T. Kim ¹⁴⁰, K. Kimura ⁹³, S. Kirsch ⁶⁵, I. Kisel ³⁹, S. Kiselev ¹⁴², A. Kisiel ¹³⁷, J.P. Kitowski ², J.L. Klay ⁵, J. Klein ³³, S. Klein ⁷⁵, C. Klein-Bösing ¹²⁷, M. Kleiner ⁶⁵, T. Klemenz ⁹⁶, A. Kluge ³³, C. Kobdaj ¹⁰⁶, T. Kollegger ⁹⁸, A. Kondratyev ¹⁴³, N. Kondratyeva ¹⁴², J. König ⁶⁵, S.A. Königstorfer ⁹⁶, P.J. Konopka ³³, G. Kornakov ¹³⁷, M. Korwieser ⁹⁶, S.D. Koryciak ², A. Kotliarov ⁸⁷, N. Kovacic ⁹⁰, V. Kovalenko ¹⁴², M. Kowalski ¹⁰⁸, V. Kozuharov ³⁷, I. Králik ⁶¹, A. Kravčáková ³⁸, L. Krcal ^{33,39}, M. Krivda ^{101,61}, F. Krizek ⁸⁷, K. Krizkova Gajdosova ³³, M. Kroesen ⁹⁵, M. Krüger ⁶⁵, D.M. Krupova ³⁶, E. Kryshen ¹⁴², V. Kučera ⁵⁹, C. Kuhn ¹³⁰, P.G. Kuijter ^{1,85}, T. Kumaoka ¹²⁶, D. Kumar ¹³⁶, L. Kumar ⁹¹, N. Kumar ⁹¹, S. Kumar ³², S. Kundu ³³, P. Kurashvili ⁸⁰, A. Kurepin ¹⁴², A.B. Kurepin ¹⁴², A. Kuryakin ¹⁴², S. Kushpil ⁸⁷, V. Kuskov ¹⁴², M. Kutyla ¹³⁷, M.J. Kweon ⁵⁹, Y. Kwon ¹⁴⁰, S.L. La Pointe ³⁹, P. La Rocca ²⁷, A. Lakrathok ¹⁰⁶, M. Lamanna ³³, A.R. Landou ⁷⁴, R. Langoy ¹²², P. Larionov ³³, E. Laudi ³³, L. Lautner ^{33,96}, R. Lavicka ¹⁰³, R. Lea ^{135,56}, H. Lee ¹⁰⁵, I. Legrand ⁴⁶, G. Legras ¹²⁷, J. Lehrbach ³⁹, T.M. Lelek ², R.C. Lemmon ^{1,86}, I. León Monzón ¹¹⁰, M.M. Lesch ⁹⁶, E.D. Lesser ¹⁹, P. Lévai ⁴⁷, X. Li ¹⁰, B.E. Liang-Gilman ¹⁹, J. Lien ¹²², R. Lietava ¹⁰¹, I. Likmeta ¹¹⁷, B. Lim ²⁵, S.H. Lim ¹⁷, V. Lindenstruth ³⁹, A. Lindner ⁴⁶, C. Lippmann ⁹⁸, D.H. Liu ⁶, J. Liu ¹²⁰, G.S.S. Liveraro ¹¹², I.M. Lofnes ²¹, C. Loizides ⁸⁸, S. Lokos ¹⁰⁸, J. Lömker ⁶⁰, P. Loncar ³⁴, X. Lopez ¹²⁸, E. López Torres ⁷, P. Lu ^{98,121}, F.V. Lugo ⁶⁸, J.R. Luhder ¹²⁷, M. Lunardon ²⁸, G. Luparello ⁵⁸, Y.G. Ma ⁴⁰, M. Mager ³³, A. Maire ¹³⁰, E.M. Majerz ², M.V. Makariev ³⁷, M. Malaev ¹⁴², G. Malfattore ²⁶, N.M. Malik ⁹², Q.W. Malik ²⁰, S.K. Malik ⁹², L. Malinina ^{I,VIII,143}, D. Mallick ^{132,81}, N. Mallick ⁴⁹, G. Mandaglio ^{31,54}, S.K. Mandal ⁸⁰, V. Manko ¹⁴², F. Manso ¹²⁸, V. Manzari ⁵¹, Y. Mao ⁶, R.W. Marcjan ², G.V. Margagliotti ²⁴, A. Margotti ⁵², A. Marín ⁹⁸, C. Markert ¹⁰⁹, P. Martinengo ³³, M.I. Martínez ⁴⁵, G. Martínez García ¹⁰⁴, M.P.P. Martins ¹¹¹, S. Masciocchi ⁹⁸, M. Masera ²⁵, A. Masoni ⁵³, L. Massacrier ¹³², O. Massen ⁶⁰, A. Mastroserio ^{133,51}, O. Matonoha ⁷⁶, S. Mattiazzo ²⁸, A. Matyja ¹⁰⁸, C. Mayer ¹⁰⁸, A.L. Mazuecos ³³, F. Mazzaschi ²⁵, M. Mazzilli ³³, J.E. Mdhuli ¹²⁴, Y. Melikyan ⁴⁴, A. Menchaca-Rocha ⁶⁸, J.E.M. Mendez ⁶⁶, E. Meninno ¹⁰³, A.S. Menon ¹¹⁷, M. Meres ¹³, Y. Miake ¹²⁶, L. Micheletti ³³, D.L. Mihaylov ⁹⁶, K. Mikhaylov ^{143,142}, D. Miśkowiec ⁹⁸, A. Modak ⁴, B. Mohanty ⁸¹, M. Mohisin Khan ^{VI,16}, M.A. Molander ⁴⁴, S. Monira ¹³⁷, C. Mordasini ¹¹⁸, D.A. Moreira De Godoy ¹²⁷, I. Morozov ¹⁴², A. Morsch ³³, T. Mrnjavac ³³, V. Muccifora ⁵⁰, S. Muhuri ¹³⁶, J.D. Mulligan ⁷⁵, A. Mulliri ²³, M.G. Munhoz ¹¹¹, R.H. Munzer ⁶⁵, H. Murakami ¹²⁵, S. Murray ¹¹⁵, L. Musa ³³, J. Musinsky ⁶¹, J.W. Myrcha ¹³⁷, B. Naik ¹²⁴, A.I. Nambrath ¹⁹, B.K. Nandi ⁴⁸, R. Nania ⁵², E. Nappi ⁵¹, A.F. Nassirpour ¹⁸, A. Nath ⁹⁵, C. Nattrass ¹²³, M.N. Naydenov ³⁷, A. Neagu ²⁰, A. Negru ¹¹⁴, E. Nekrasova ¹⁴², L. Nellen ⁶⁶, R. Nepeivoda ⁷⁶, S. Nese ²⁰, G. Neskovic ³⁹, N. Nicassio ⁵¹, B.S. Nielsen ⁸⁴, E.G. Nielsen ⁸⁴, S. Nikolaev ¹⁴², S. Nikulin ¹⁴², V. Nikulin ¹⁴², F. Noferini ⁵², S. Noh ¹², P. Nomokonov ¹⁴³, J. Norman ¹²⁰, N. Novitzky ⁸⁸, P. Nowakowski ¹³⁷, A. Nyanin ¹⁴², J. Nystrand ²¹, S. Oh ¹⁸, A. Ohlson ⁷⁶, V.A. Okorokov ¹⁴², J. Olienczak ¹³⁷, A. Onnerstad ¹¹⁸, C. Oppedisano ⁵⁷, A. Ortiz Velasquez ⁶⁶, J. Otwinowski ¹⁰⁸, M. Oya ⁹³, K. Oyama ⁷⁷, Y. Pachmayer ⁹⁵, S. Padhan ⁴⁸, D. Pagano ^{135,56}, G. Paic ⁶⁶, S. Paisano-Guzmán ⁴⁵, A. Palasciano ⁵¹, S. Panebianco ¹³¹, H. Park ¹²⁶, H. Park ¹⁰⁵, J. Park ⁵⁹, J.E. Parkkila ³³, Y. Patley ⁴⁸,

B. Paul ²³, M.M.D.M. Paulino ¹¹¹, H. Pei ⁶, T. Peitzmann ⁶⁰, X. Peng ¹¹, M. Pennisi ²⁵,
 S. Perciballi ²⁵, D. Peresunko ¹⁴², G.M. Perez ⁷, Y. Pestov ¹⁴², V. Petrov ¹⁴², M. Petrovici ⁴⁶,
 R.P. Pezzi ^{104,67}, S. Piano ⁵⁸, M. Pikna ¹³, P. Pillot ¹⁰⁴, O. Pinazza ^{52,33}, L. Pinsky ¹¹⁷, C. Pinto ⁹⁶,
 S. Pisano ⁵⁰, M. Płoskoń ⁷⁵, M. Planinic ⁹⁰, F. Pliquett ⁶⁵, M.G. Poghosyan ⁸⁸, B. Polichtchouk ¹⁴²,
 S. Politano ³⁰, N. Poljak ⁹⁰, A. Pop ⁴⁶, S. Porteboeuf-Houssais ¹²⁸, V. Pozdniakov ¹⁴³, I.Y. Pozos ⁴⁵,
 K.K. Pradhan ⁴⁹, S.K. Prasad ⁴, S. Prasad ⁴⁹, R. Preghenella ⁵², F. Prino ⁵⁷, C.A. Pruneau ¹³⁸,
 I. Pshenichnov ¹⁴², M. Puccio ³³, S. Pucillo ²⁵, Z. Pugelova ¹⁰⁷, S. Qiu ⁸⁵, L. Quaglia ²⁵, S. Ragoni ¹⁵,
 A. Rai ¹³⁹, A. Rakotozafindrabe ¹³¹, L. Ramello ^{134,57}, F. Rami ¹³⁰, T.A. Rancien ⁷⁴, M. Rasa ²⁷,
 S.S. Räsänen ⁴⁴, R. Rath ⁵², M.P. Rauch ²¹, I. Ravasenga ³³, K.F. Read ^{88,123}, C. Reckziegel ¹¹³,
 A.R. Redelbach ³⁹, K. Redlich ^{VII,80}, C.A. Reetz ⁹⁸, H.D. Regules-Medel ⁴⁵, A. Rehman ²¹, F. Reidt ³³,
 H.A. Reme-Ness ³⁵, Z. Rescakova ³⁸, K. Reygers ⁹⁵, A. Riabov ¹⁴², V. Riabov ¹⁴², R. Ricci ²⁹,
 M. Richter ²⁰, A.A. Riedel ⁹⁶, W. Riegler ³³, A.G. Riffero ²⁵, C. Ristea ⁶⁴, M.V. Rodriguez ³³,
 M. Rodríguez Cahuantzi ⁴⁵, S.A. Rodríguez Ramírez ⁴⁵, K. Røed ²⁰, R. Rogalev ¹⁴², E. Rogochaya ¹⁴³,
 T.S. Rogoschinski ⁶⁵, D. Rohr ³³, D. Röhrich ²¹, P.F. Rojas ⁴⁵, S. Rojas Torres ³⁶, P.S. Rokita ¹³⁷,
 G. Romanenko ²⁶, F. Ronchetti ⁵⁰, A. Rosano ^{31,54}, E.D. Rosas ⁶⁶, K. Roslon ¹³⁷, A. Rossi ⁵⁵,
 A. Roy ⁴⁹, S. Roy ⁴⁸, N. Rubini ²⁶, D. Ruggiano ¹³⁷, R. Rui ²⁴, P.G. Russek ², R. Russo ⁸⁵,
 A. Rustamov ⁸², E. Ryabinkin ¹⁴², Y. Ryabov ¹⁴², A. Rybicki ¹⁰⁸, H. Rytönen ¹¹⁸, J. Ryu ¹⁷,
 W. Rzesza ¹³⁷, O.A.M. Saarimäki ⁴⁴, S. Sadhu ³², S. Sadosky ¹⁴², J. Saetre ²¹, K. Šafařík ³⁶, P. Saha ⁴²,
 S.K. Saha ⁴, S. Saha ⁸¹, B. Sahoo ⁴⁸, B. Sahoo ⁴⁹, R. Sahoo ⁴⁹, S. Sahoo ⁶², D. Sahu ⁴⁹, P.K. Sahu ⁶²,
 J. Saini ¹³⁶, K. Sajdakova ³⁸, S. Sakai ¹²⁶, M.P. Salvan ⁹⁸, S. Sambyal ⁹², D. Samitz ¹⁰³, I. Sanna ^{33,96},
 T.B. Saramela ¹¹¹, D. Sarkar ⁸⁴, P. Sarma ⁴², V. Sarritzu ²³, V.M. Sarti ⁹⁶, M.H.P. Sas ³³, S. Sawan ⁸¹,
 E. Scapparone ⁵², J. Schambach ⁸⁸, H.S. Scheid ⁶⁵, C. Schiaua ⁴⁶, R. Schicker ⁹⁵, F. Schlepfer ⁹⁵,
 A. Schmah ⁹⁸, C. Schmidt ⁹⁸, H.R. Schmidt ⁹⁴, M.O. Schmidt ³³, M. Schmidt ⁹⁴, N.V. Schmidt ⁸⁸,
 A.R. Schmier ¹²³, R. Schotter ¹³⁰, A. Schröter ³⁹, J. Schukraft ³³, K. Schweda ⁹⁸, G. Scioli ²⁶,
 E. Scomparin ⁵⁷, J.E. Seger ¹⁵, Y. Sekiguchi ¹²⁵, D. Sekihata ¹²⁵, M. Selina ⁸⁵, I. Selyuzhenkov ⁹⁸,
 S. Senyukov ¹³⁰, J.J. Seo ⁹⁵, D. Serebryakov ¹⁴², L. Serkin ⁶⁶, L. Šerkšnytė ⁹⁶, A. Sevcenco ⁶⁴,
 T.J. Shaba ⁶⁹, A. Shabetai ¹⁰⁴, R. Shahoyan ³³, A. Shangaraev ¹⁴², B. Sharma ⁹², D. Sharma ⁴⁸,
 H. Sharma ⁵⁵, M. Sharma ⁹², S. Sharma ⁷⁷, S. Sharma ⁹², U. Sharma ⁹², A. Shatat ¹³², O. Sheibani ¹¹⁷,
 K. Shigaki ⁹³, M. Shimomura ⁷⁸, J. Shin ¹², S. Shirinkin ¹⁴², Q. Shou ⁴⁰, Y. Sibiriak ¹⁴², S. Siddhanta ⁵³,
 T. Siemiarczuk ⁸⁰, T.F. Silva ¹¹¹, D. Silvermyr ⁷⁶, T. Simantathammakul ¹⁰⁶, R. Simeonov ³⁷, B. Singh ⁹²,
 B. Singh ⁹⁶, K. Singh ⁴⁹, R. Singh ⁸¹, R. Singh ⁹², R. Singh ^{98,49}, S. Singh ¹⁶, V.K. Singh ¹³⁶,
 V. Singhal ¹³⁶, T. Sinha ¹⁰⁰, B. Sitar ¹³, M. Sitta ^{134,57}, T.B. Skaali ²⁰, G. Skorodumovs ⁹⁵,
 M. Slupecki ⁴⁴, N. Smirnov ¹³⁹, R.J.M. Snellings ⁶⁰, E.H. Solheim ²⁰, J. Song ¹⁷, C. Sonnabend ^{33,98},
 J.M. Sonneveld ⁸⁵, F. Soramel ²⁸, A.B. Soto-Hernandez ⁸⁹, R. Spijkers ⁸⁵, I. Sputowska ¹⁰⁸, J. Staa ⁷⁶,
 J. Stachel ⁹⁵, I. Stan ⁶⁴, P.J. Steffanic ¹²³, S.F. Stiefelmaier ⁹⁵, D. Stocco ¹⁰⁴, I. Storehaug ²⁰,
 P. Stratmann ¹²⁷, S. Strazzi ²⁶, A. Sturmiolo ^{31,54}, C.P. Stylianidis ⁸⁵, A.A.P. Suaide ¹¹¹, C. Suire ¹³²,
 M. Sukhanov ¹⁴², M. Suljic ³³, R. Sultanov ¹⁴², V. Sumberia ⁹², S. Sumowidagdo ⁸³, I. Szarka ¹³,
 M. Szymkowski ¹³⁷, S.F. Taghavi ⁹⁶, G. Taillepied ⁹⁸, J. Takahashi ¹¹², G.J. Tambave ⁸¹, S. Tang ⁶,
 Z. Tang ¹²¹, J.D. Tapia Takaki ¹¹⁹, N. Tapus ¹¹⁴, L.A. Tarasovicova ¹²⁷, M.G. Tazila ⁴⁶, G.F. Tassielli ³²,
 A. Tauro ³³, A. Tavira García ¹³², G. Tejeda Muñoz ⁴⁵, A. Telesca ³³, L. Terlizzi ²⁵, C. Terrevoli ¹¹⁷,
 S. Thakur ⁴, D. Thomas ¹⁰⁹, A. Tikhonov ¹⁴², N. Tiltmann ¹²⁷, A.R. Timmins ¹¹⁷, M. Tkacik ¹⁰⁷,
 T. Tkacik ¹⁰⁷, A. Toia ⁶⁵, R. Tokumoto ⁹³, K. Tomohiro ⁹³, N. Topilskaya ¹⁴², M. Toppi ⁵⁰, T. Tork ¹³²,
 V.V. Torres ¹⁰⁴, A.G. Torres Ramos ³², A. Trifiro ^{31,54}, A.S. Triolo ^{33,31,54}, S. Tripathy ⁵²,
 T. Tripathy ⁴⁸, S. Trogolo ³³, V. Trubnikov ³, W.H. Trzaska ¹¹⁸, T.P. Trzcinski ¹³⁷, A. Tumkin ¹⁴²,
 R. Turrisi ⁵⁵, T.S. Tveter ²⁰, K. Ullaland ²¹, B. Ulukutlu ⁹⁶, A. Uras ¹²⁹, M. Urioni ¹³⁵, G.L. Usai ²³,
 M. Vala ³⁸, N. Valle ²², L.V.R. van Doremalen ⁶⁰, M. van Leeuwen ⁸⁵, C.A. van Veen ⁹⁵, R.J.G. van
 Weelden ⁸⁵, P. Vande Vyvre ³³, D. Varga ⁴⁷, Z. Varga ⁴⁷, P. Vargas Torres ⁶⁶, M. Vasileiou ⁷⁹,
 A. Vasiliev ¹⁴², O. Vázquez Doce ⁵⁰, O. Vazquez Rueda ¹¹⁷, V. Vechernin ¹⁴², E. Vercellin ²⁵, S. Vergara
 Limón ⁴⁵, R. Verma ⁴⁸, L. Vermunt ⁹⁸, R. Vértesi ⁴⁷, M. Verweij ⁶⁰, L. Vickovic ³⁴, Z. Vilakazi ¹²⁴,
 O. Villalobos Baillie ¹⁰¹, A. Villani ²⁴, A. Vinogradov ¹⁴², T. Virgili ²⁹, M.M.O. Virta ¹¹⁸,
 V. Vislavicius ⁷⁶, A. Vodopyanov ¹⁴³, B. Volkel ³³, M.A. Völkl ⁹⁵, S.A. Voloshin ¹³⁸, G. Volpe ³², B. von
 Haller ³³, I. Vorobyev ³³, N. Vozniuk ¹⁴², J. Vrláková ³⁸, J. Wan ⁴⁰, C. Wang ⁴⁰, D. Wang ⁴⁰,
 Y. Wang ⁴⁰, Y. Wang ⁶, A. Wegrzynek ³³, F.T. Weiglhofer ³⁹, S.C. Wenzel ³³, J.P. Wessels ¹²⁷,
 J. Wiechula ⁶⁵, J. Wikne ²⁰, G. Wilk ⁸⁰, J. Wilkinson ⁹⁸, G.A. Willems ¹²⁷, B. Windelband ⁹⁵,
 M. Winn ¹³¹, J.R. Wright ¹⁰⁹, W. Wu ⁴⁰, Y. Wu ¹²¹, Z. Xiong ¹²¹, R. Xu ⁶, A. Yadav ⁴³, A.K. Yadav ¹³⁶,
 S. Yalcin ⁷³, Y. Yamaguchi ⁹³, S. Yang ²¹, S. Yano ⁹³, E.R. Yeats ¹⁹, Z. Yin ⁶, I.-K. Yoo ¹⁷, J.H. Yoon ⁵⁹,

H. Yu¹², S. Yuan²¹, A. Yuncu⁹⁵, V. Zaccaro²⁴, C. Zampolli³³, F. Zanone⁹⁵, N. Zardoshti³³,
 A. Zarochentsev¹⁴², P. Závada⁶³, N. Zaviyalov¹⁴², M. Zhalov¹⁴², B. Zhang⁶, C. Zhang¹³¹,
 L. Zhang⁴⁰, M. Zhang⁶, S. Zhang⁴⁰, X. Zhang⁶, Y. Zhang¹²¹, Z. Zhang⁶, M. Zhao¹⁰,
 V. Zhrebchevskii¹⁴², Y. Zhi¹⁰, C. Zhong⁴⁰, D. Zhou⁶, Y. Zhou⁸⁴, J. Zhu^{55,6}, Y. Zhu⁶,
 S.C. Zugeravel⁵⁷, N. Zurlo^{135,56}

Affiliation Notes

^I Deceased

^{II} Also at: Max-Planck-Institut für Physik, Munich, Germany

^{III} Also at: Italian National Agency for New Technologies, Energy and Sustainable Economic Development (ENEA), Bologna, Italy

^{IV} Also at: Dipartimento DET del Politecnico di Torino, Turin, Italy

^V Also at: Yildiz Technical University, Istanbul, Türkiye

^{VI} Also at: Department of Applied Physics, Aligarh Muslim University, Aligarh, India

^{VII} Also at: Institute of Theoretical Physics, University of Wrocław, Poland

^{VIII} Also at: An institution covered by a cooperation agreement with CERN

Collaboration Institutes

¹ A.I. Alikhanyan National Science Laboratory (Yerevan Physics Institute) Foundation, Yerevan, Armenia

² AGH University of Krakow, Cracow, Poland

³ Bogolyubov Institute for Theoretical Physics, National Academy of Sciences of Ukraine, Kiev, Ukraine

⁴ Bose Institute, Department of Physics and Centre for Astroparticle Physics and Space Science (CAPSS), Kolkata, India

⁵ California Polytechnic State University, San Luis Obispo, California, United States

⁶ Central China Normal University, Wuhan, China

⁷ Centro de Aplicaciones Tecnológicas y Desarrollo Nuclear (CEADEN), Havana, Cuba

⁸ Centro de Investigación y de Estudios Avanzados (CINVESTAV), Mexico City and Mérida, Mexico

⁹ Chicago State University, Chicago, Illinois, United States

¹⁰ China Institute of Atomic Energy, Beijing, China

¹¹ China University of Geosciences, Wuhan, China

¹² Chungbuk National University, Cheongju, Republic of Korea

¹³ Comenius University Bratislava, Faculty of Mathematics, Physics and Informatics, Bratislava, Slovak Republic

¹⁴ COMSATS University Islamabad, Islamabad, Pakistan

¹⁵ Creighton University, Omaha, Nebraska, United States

¹⁶ Department of Physics, Aligarh Muslim University, Aligarh, India

¹⁷ Department of Physics, Pusan National University, Pusan, Republic of Korea

¹⁸ Department of Physics, Sejong University, Seoul, Republic of Korea

¹⁹ Department of Physics, University of California, Berkeley, California, United States

²⁰ Department of Physics, University of Oslo, Oslo, Norway

²¹ Department of Physics and Technology, University of Bergen, Bergen, Norway

²² Dipartimento di Fisica, Università di Pavia, Pavia, Italy

²³ Dipartimento di Fisica dell'Università and Sezione INFN, Cagliari, Italy

²⁴ Dipartimento di Fisica dell'Università and Sezione INFN, Trieste, Italy

²⁵ Dipartimento di Fisica dell'Università and Sezione INFN, Turin, Italy

²⁶ Dipartimento di Fisica e Astronomia dell'Università and Sezione INFN, Bologna, Italy

²⁷ Dipartimento di Fisica e Astronomia dell'Università and Sezione INFN, Catania, Italy

²⁸ Dipartimento di Fisica e Astronomia dell'Università and Sezione INFN, Padova, Italy

²⁹ Dipartimento di Fisica 'E.R. Caianiello' dell'Università and Gruppo Collegato INFN, Salerno, Italy

³⁰ Dipartimento DISAT del Politecnico and Sezione INFN, Turin, Italy

³¹ Dipartimento di Scienze MIIFT, Università di Messina, Messina, Italy

³² Dipartimento Interateneo di Fisica 'M. Merlin' and Sezione INFN, Bari, Italy

³³ European Organization for Nuclear Research (CERN), Geneva, Switzerland

³⁴ Faculty of Electrical Engineering, Mechanical Engineering and Naval Architecture, University of Split, Split, Croatia

- ³⁵ Faculty of Engineering and Science, Western Norway University of Applied Sciences, Bergen, Norway
- ³⁶ Faculty of Nuclear Sciences and Physical Engineering, Czech Technical University in Prague, Prague, Czech Republic
- ³⁷ Faculty of Physics, Sofia University, Sofia, Bulgaria
- ³⁸ Faculty of Science, P.J. Šafárik University, Košice, Slovak Republic
- ³⁹ Frankfurt Institute for Advanced Studies, Johann Wolfgang Goethe-Universität Frankfurt, Frankfurt, Germany
- ⁴⁰ Fudan University, Shanghai, China
- ⁴¹ Gangneung-Wonju National University, Gangneung, Republic of Korea
- ⁴² Gauhati University, Department of Physics, Guwahati, India
- ⁴³ Helmholtz-Institut für Strahlen- und Kernphysik, Rheinische Friedrich-Wilhelms-Universität Bonn, Bonn, Germany
- ⁴⁴ Helsinki Institute of Physics (HIP), Helsinki, Finland
- ⁴⁵ High Energy Physics Group, Universidad Autónoma de Puebla, Puebla, Mexico
- ⁴⁶ Horia Hulubei National Institute of Physics and Nuclear Engineering, Bucharest, Romania
- ⁴⁷ HUN-REN Wigner Research Centre for Physics, Budapest, Hungary
- ⁴⁸ Indian Institute of Technology Bombay (IIT), Mumbai, India
- ⁴⁹ Indian Institute of Technology Indore, Indore, India
- ⁵⁰ INFN, Laboratori Nazionali di Frascati, Frascati, Italy
- ⁵¹ INFN, Sezione di Bari, Bari, Italy
- ⁵² INFN, Sezione di Bologna, Bologna, Italy
- ⁵³ INFN, Sezione di Cagliari, Cagliari, Italy
- ⁵⁴ INFN, Sezione di Catania, Catania, Italy
- ⁵⁵ INFN, Sezione di Padova, Padova, Italy
- ⁵⁶ INFN, Sezione di Pavia, Pavia, Italy
- ⁵⁷ INFN, Sezione di Torino, Turin, Italy
- ⁵⁸ INFN, Sezione di Trieste, Trieste, Italy
- ⁵⁹ Inha University, Incheon, Republic of Korea
- ⁶⁰ Institute for Gravitational and Subatomic Physics (GRASP), Utrecht University/Nikhef, Utrecht, Netherlands
- ⁶¹ Institute of Experimental Physics, Slovak Academy of Sciences, Košice, Slovak Republic
- ⁶² Institute of Physics, Homi Bhabha National Institute, Bhubaneswar, India
- ⁶³ Institute of Physics of the Czech Academy of Sciences, Prague, Czech Republic
- ⁶⁴ Institute of Space Science (ISS), Bucharest, Romania
- ⁶⁵ Institut für Kernphysik, Johann Wolfgang Goethe-Universität Frankfurt, Frankfurt, Germany
- ⁶⁶ Instituto de Ciencias Nucleares, Universidad Nacional Autónoma de México, Mexico City, Mexico
- ⁶⁷ Instituto de Física, Universidade Federal do Rio Grande do Sul (UFRGS), Porto Alegre, Brazil
- ⁶⁸ Instituto de Física, Universidad Nacional Autónoma de México, Mexico City, Mexico
- ⁶⁹ iThemba LABS, National Research Foundation, Somerset West, South Africa
- ⁷⁰ Jeonbuk National University, Jeonju, Republic of Korea
- ⁷¹ Johann-Wolfgang-Goethe Universität Frankfurt Institut für Informatik, Fachbereich Informatik und Mathematik, Frankfurt, Germany
- ⁷² Korea Institute of Science and Technology Information, Daejeon, Republic of Korea
- ⁷³ KTO Karatay University, Konya, Turkey
- ⁷⁴ Laboratoire de Physique Subatomique et de Cosmologie, Université Grenoble-Alpes, CNRS-IN2P3, Grenoble, France
- ⁷⁵ Lawrence Berkeley National Laboratory, Berkeley, California, United States
- ⁷⁶ Lund University Department of Physics, Division of Particle Physics, Lund, Sweden
- ⁷⁷ Nagasaki Institute of Applied Science, Nagasaki, Japan
- ⁷⁸ Nara Women's University (NWU), Nara, Japan
- ⁷⁹ National and Kapodistrian University of Athens, School of Science, Department of Physics, Athens, Greece
- ⁸⁰ National Centre for Nuclear Research, Warsaw, Poland
- ⁸¹ National Institute of Science Education and Research, Homi Bhabha National Institute, Jatni, India
- ⁸² National Nuclear Research Center, Baku, Azerbaijan
- ⁸³ National Research and Innovation Agency - BRIN, Jakarta, Indonesia
- ⁸⁴ Niels Bohr Institute, University of Copenhagen, Copenhagen, Denmark
- ⁸⁵ Nikhef, National institute for subatomic physics, Amsterdam, Netherlands
- ⁸⁶ Nuclear Physics Group, STFC Daresbury Laboratory, Daresbury, United Kingdom

- 87 Nuclear Physics Institute of the Czech Academy of Sciences, Husinec-Řež, Czech Republic
- 88 Oak Ridge National Laboratory, Oak Ridge, Tennessee, United States
- 89 Ohio State University, Columbus, Ohio, United States
- 90 Physics department, Faculty of science, University of Zagreb, Zagreb, Croatia
- 91 Physics Department, Panjab University, Chandigarh, India
- 92 Physics Department, University of Jammu, Jammu, India
- 93 Physics Program and International Institute for Sustainability with Knotted Chiral Meta Matter (SKCM2), Hiroshima University, Hiroshima, Japan
- 94 Physikalisches Institut, Eberhard-Karls-Universität Tübingen, Tübingen, Germany
- 95 Physikalisches Institut, Ruprecht-Karls-Universität Heidelberg, Heidelberg, Germany
- 96 Physik Department, Technische Universität München, Munich, Germany
- 97 Politecnico di Bari and Sezione INFN, Bari, Italy
- 98 Research Division and ExtreMe Matter Institute EMMI, GSI Helmholtzzentrum für Schwerionenforschung GmbH, Darmstadt, Germany
- 99 Saga University, Saga, Japan
- 100 Saha Institute of Nuclear Physics, Homi Bhabha National Institute, Kolkata, India
- 101 School of Physics and Astronomy, University of Birmingham, Birmingham, United Kingdom
- 102 Sección Física, Departamento de Ciencias, Pontificia Universidad Católica del Perú, Lima, Peru
- 103 Stefan Meyer Institut für Subatomare Physik (SMI), Vienna, Austria
- 104 SUBATECH, IMT Atlantique, Nantes Université, CNRS-IN2P3, Nantes, France
- 105 Sungkyunkwan University, Suwon City, Republic of Korea
- 106 Suranaree University of Technology, Nakhon Ratchasima, Thailand
- 107 Technical University of Košice, Košice, Slovak Republic
- 108 The Henryk Niewodniczanski Institute of Nuclear Physics, Polish Academy of Sciences, Cracow, Poland
- 109 The University of Texas at Austin, Austin, Texas, United States
- 110 Universidad Autónoma de Sinaloa, Culiacán, Mexico
- 111 Universidade de São Paulo (USP), São Paulo, Brazil
- 112 Universidade Estadual de Campinas (UNICAMP), Campinas, Brazil
- 113 Universidade Federal do ABC, Santo Andre, Brazil
- 114 Universitatea Nationala de Stiinta si Tehnologie Politehnica Bucuresti, Bucharest, Romania
- 115 University of Cape Town, Cape Town, South Africa
- 116 University of Derby, Derby, United Kingdom
- 117 University of Houston, Houston, Texas, United States
- 118 University of Jyväskylä, Jyväskylä, Finland
- 119 University of Kansas, Lawrence, Kansas, United States
- 120 University of Liverpool, Liverpool, United Kingdom
- 121 University of Science and Technology of China, Hefei, China
- 122 University of South-Eastern Norway, Kongsberg, Norway
- 123 University of Tennessee, Knoxville, Tennessee, United States
- 124 University of the Witwatersrand, Johannesburg, South Africa
- 125 University of Tokyo, Tokyo, Japan
- 126 University of Tsukuba, Tsukuba, Japan
- 127 Universität Münster, Institut für Kernphysik, Münster, Germany
- 128 Université Clermont Auvergne, CNRS/IN2P3, LPC, Clermont-Ferrand, France
- 129 Université de Lyon, CNRS/IN2P3, Institut de Physique des 2 Infinis de Lyon, Lyon, France
- 130 Université de Strasbourg, CNRS, IPHC UMR 7178, F-67000 Strasbourg, France, Strasbourg, France
- 131 Université Paris-Saclay, Centre d'Etudes de Saclay (CEA), IRFU, Département de Physique Nucléaire (DPhN), Saclay, France
- 132 Université Paris-Saclay, CNRS/IN2P3, IJCLab, Orsay, France
- 133 Università degli Studi di Foggia, Foggia, Italy
- 134 Università del Piemonte Orientale, Vercelli, Italy
- 135 Università di Brescia, Brescia, Italy
- 136 Variable Energy Cyclotron Centre, Homi Bhabha National Institute, Kolkata, India
- 137 Warsaw University of Technology, Warsaw, Poland
- 138 Wayne State University, Detroit, Michigan, United States
- 139 Yale University, New Haven, Connecticut, United States

¹⁴⁰ Yonsei University, Seoul, Republic of Korea

¹⁴¹ Zentrum für Technologie und Transfer (ZTT), Worms, Germany

¹⁴² Affiliated with an institute covered by a cooperation agreement with CERN

¹⁴³ Affiliated with an international laboratory covered by a cooperation agreement with CERN.